CZ-tope at Susquehanna Shale Hills CZO: Synthesizing multiple isotope proxies to elucidate Critical Zone processes across timescales in a temperate forested landscape

Article · May 2016

DOI: 10.1016/j.chemgeo.2016.05.012

14 authors, including:

Pamela L. Sullivan

University of Kansas

23 PUBLICATIONS **119** CITATIONS

SEE PROFILE

David M Eissenstat

Pennsylvania State University

171 PUBLICATIONS **7,609** CITATIONS

SEE PROFILE

Jérôme Gaillardet

Institut de Physique du Globe de Paris

218 PUBLICATIONS **8,154** CITATIONS

SEE PROFILE

Susan L. Brantley

Pennsylvania State University

396 PUBLICATIONS **12,465** CITATIONS

SEE PROFILE

Chemical Geology xxx (2016) xxx–xxx

Contents lists available at ScienceDirect

Chemical Geology

journal homepage: www.elsevier.com/locate/chemgeo

CZ-tope at Susquehanna Shale Hills CZO: Synthesizing multiple isotope proxies to elucidate Critical Zone processes across timescales in a temperate forested landscape

P.L. Sullivan [a,b,*], L. Ma [c], N. West [a,d], L. Jin [c], D.L. Karwan [e], J. Noireaux [f], G. Steinhoefel [a], K.P. Gaines [g], D.M. Eissenstat [g], J. Gaillardet [f], L.A. Derry [h], K. Meek [h], S. Hynek [a], S.L. Brantley [a]

[a] Earth and Environmental Systems Institute and Department of Geosciences, Pennsylvania State University, State College, PA, USA
[b] Department of Geography and Atmospheric Science, University of Kansas, Lawrence, KS, USA
[c] Department of Geological Sciences, University of Texas El Paso, El Paso, TX, USA
[d] Earth and Atmospheric Sciences, Georgia Institute of Technology, Atlanta, GA, USA
[e] Department of Forest Resources, University of Minnesota, Saint Paul, MN, USA
[f] Institut de Physique du Globe de Paris, Sorbonne Paris Cité, Université Paris Diderot, Paris, France
[g] Department of Ecosystem Science and Management, Pennsylvania State University, State College, PA, USA
[h] Department of Earth and Atmospheric Sciences, Cornell University, Ithaca, NY, USA

ARTICLE INFO

Article history:
Received 22 October 2015
Received in revised form 11 May 2016
Accepted 16 May 2016
Available online xxxx

Keywords:
Isotopes
Weathering
Critical Zone
Regolith
Landscape evolution
Shale

ABSTRACT

The application of multiple isotope proxies on the same location within a Critical Zone (CZ), which we term "CZ-tope", elucidates the interactions of geochemical, geomorphological, hydrological and biological processes together with anthropogenic influences in the CZ across widely disparate timescales. We exemplify the CZ-tope approach by summarizing the emerging hypotheses developed from isotopic measurements at the Susquehanna Shale Hills CZ Observatory (SSHCZO), Pennsylvania (U.S.A).

At SSHCZO, measurements of U-series isotopes and meteoric ^{10}Be in regolith provide evidence that the catchment is approaching a steady state at the ridgetops where regolith production is balanced by erosive loss. Isotopic measurements of δ^{13}C, ^{87}Sr/^{86}Sr, and δ^{34}S in the regolith, bedrock and water, together with ^{3}H, δ^{2}H and δ^{18}O in various water reservoirs (precipitation, soil water, stream water and groundwater) support the hypothesis that nested reaction fronts have developed in the subsurface over timescales of millennia. Combinations of U-series and meteoric ^{10}Be in bedrock and regolith and measurements of soil water δ^{18}O led to the hypothesis that freeze-thaw is the dominant soil creep mechanism controlling regolith fluxes and hillslopes. Utilizing the CZ-tope approach of measuring δ^{26}Mg, δ^{56}Fe and δ^{11}B isotopes on identical samples, we also developed a working hypothesis that particle transport in the subsurface represents a significant weathering loss from the catchment. Likewise, the use of δ^{18}O, Ge/Si and ^{87}Sr/^{86}Sr ratios in xylem source waters (precipitation, soil, stream- and ground-), along with ^{87}Sr/^{86}Sr ratios from soils, led to the hypothesis that O isotope fractionation occurs near clay surfaces. Finally, analyses of ^{206}Pb/^{204}Pb, ^{207}Pb/^{204}Pb, ^{208}Pb/^{204}Pb and ^{137}Cs in soil from hillslope profiles have also revealed the imprint of widespread human activity. CZ-tope — the interpretation of multiple elements' isotopic ratios quantified for identical samples in one landscape — thus paints an emerging picture of SSHCZO as a relatively fast-eroding but slow-weathering landscape in which: i) nutrients are tightly cycled by vegetation, ii) soils move downslope largely by freeze-thaw, iii) subsurface particle transport is an important flux for mass loss, iv) mobile and immobile reservoirs act to fractionate water and cations into trees and stream water, and v) the imprint of humans is manifested in the metal contents of the topsoil.

1. Introduction

Supporting all terrestrial life, the Critical Zone (CZ), extends from the top of the canopy down to the intersection of unweathered bedrock and the groundwater table (Brantley et al., 2007). The study of the CZ requires investigations of earth-surface processes crossing time scales of seconds to that of millennia. To cross such scales requires measurements of today's fluxes (water and solutes) and the records of those fluxes in the geologic record (soils and sediments). Within the CZ, isotopic fractionation of elements is affected by multiple processes: as such, isotopes can help fingerprint processes and quantify element fluxes

* Corresponding author at: Earth and Environmental Systems Institute and Department of Geosciences, Pennsylvania State University, State College, PA, USA.

http://dx.doi.org/10.1016/j.chemgeo.2016.05.012
0009-2541/

over a broad range of timescales. This approach is particularly helpful when researchers use multiple isotopes in the same setting to elucidate complex systems (Fig. 1, Table 1). For example, the combination of traditional O and H stable isotopes along with U-series and Sr isotopes in water has been utilized to understand catchment hydrodynamics and groundwater flow paths (Kendall and McDonnell, 2006; Maher et al., 2006). In addition, quantifying time scales of regolith formation, as well as erosion and weathering rates is possible by measuring U-series isotopes and cosmogenic nuclides in soils and sediments (e.g. ^{10}Be, ^{26}Al; Chabaux and Ma, 2011; Cockburn and Summerfield, 2004). Likewise, non-traditional stable isotope systems (e.g. Si, Mg, Ca, Fe, Li, B) are emerging as powerful tools to understand dissolution of primary minerals, the formation of secondary minerals and the influence of biological activity (e.g. Bouchez et al., 2013; Opfergelt et al., 2012a,b; Schmitt et al., 2012). Finally, isotope variations of heavy metals (e.g. Cu, Zn, Cd, Hg, and Cr) are helpful in identifying anthropogenic influences on the CZ (Bigalke et al., 2010).

While these isotope systems have been developed over the last five decades, there are only a handful of catchments worldwide where multiple isotope systems have been measured on the same samples or locations to evaluate CZ processes over multiple timescales. For example, multiple isotopes have been used to elucidate plant-water-nutrient uptake, catchment hydrodynamics, physical and chemical weathering rates, and the impact of humans in the Strengbach Catchment in North East France, the Rio Icacos catchment in Puerto Rico (U.S.A.), the mountains of Guadeloupe (France), the Damma Glacier (Switerland; Big Link Project) and locations in Hawaii (U.S.A) (Table 2). Many of these research sites have generated data sets, while not always on the exact same samples, that lend themselves to the kind of synthetic, multiple isotopic signature-derived work we call "CZ-tope". Since 1996, geochemists have grown the number of isotopic systems in use from a focus on O, S, N, C, and H to ~30 isotopic systems in use today. This has expanded the CZ-tope concept to the application of multiple isotope systems on the same samples or on identical sites (Fig. 1). To date, CZ-tope includes traditional stable isotopes (e.g., C, H, O, N, S), cosmogenic nuclides (e.g., ^{10}Be), non-traditional stable isotopes (e.g., Mg, Ca, Fe, Cu, Li, B), radiogenic isotopes (e.g., U-series, Sr, Pb), and fission products (e.g. ^{137}Cs) (Table 1).

We employ the CZ-tope approach at the Susquehanna Shale Hills Critical Zone Observatory (SSHCZO) by synthesizing isotopic research presented in earlier studies (Brantley et al., 2013; Gaines et al., 2015; Jin et al., 2014; Ma et al., 2010, 2012, 2013, 2014, 2015; Meek et al., 2016; Noireaux et al., 2014; Sullivan et al., 2016; Thomas et al., 2013; West et al., 2013, 2014; Yesavage et al., 2012) to investigate CZ processes from daily to millennial timescales. Specifically, we examine processes that govern the conversion of bedrock into regolith, downslope transport of mobile regolith, and fluxes of weathering-derived solutes. We show how the CZ-tope approach has led to a series of hypotheses that cross timescales and we focus this paper on four hypotheses: i) meteoric fluxes and surbsurface flow paths drive the development of nested reaction fronts in the SSHCZO subsurface; ii) meteoric influxes of water drive soil creep, largely by the mechanism of freeze-thaw, and soil production, largely by fracturing and chemical weathering, and results in steeper slopes on the shaded side of the catchment; iii) atmospheric deposition has imprinted soils with metals that document the industrial revolution and isotopes that document wide-spread nuclear weapons testing; and iv) soils act as valves that separate water in the clay-rich soil matrix from water in macropores so that these slow- or fast-flowing waters respectively are taken up by vegetation or recharged to the stream.

2. Susquehanna Shale Hills Critical Zone Observatory (SSHCZO)

Located in the Valley and Ridge Physiographic Province of central Pennsylvania (USA), the Susquehanna Shale Hill Critical Zone Observatory (Fig. 2; Table 3) is a small (7.9 ha), forested, first-order, V-shaped catchment developed on the Silurian Rose Hill Formation. The Rose Hill Formation is primarily comprised of shale with sandy or calcite-rich interbeds hosted by the upper half of the stratigraphic section (Flueckinger, 1969; Cotter and Inners, 1986). Shale from the

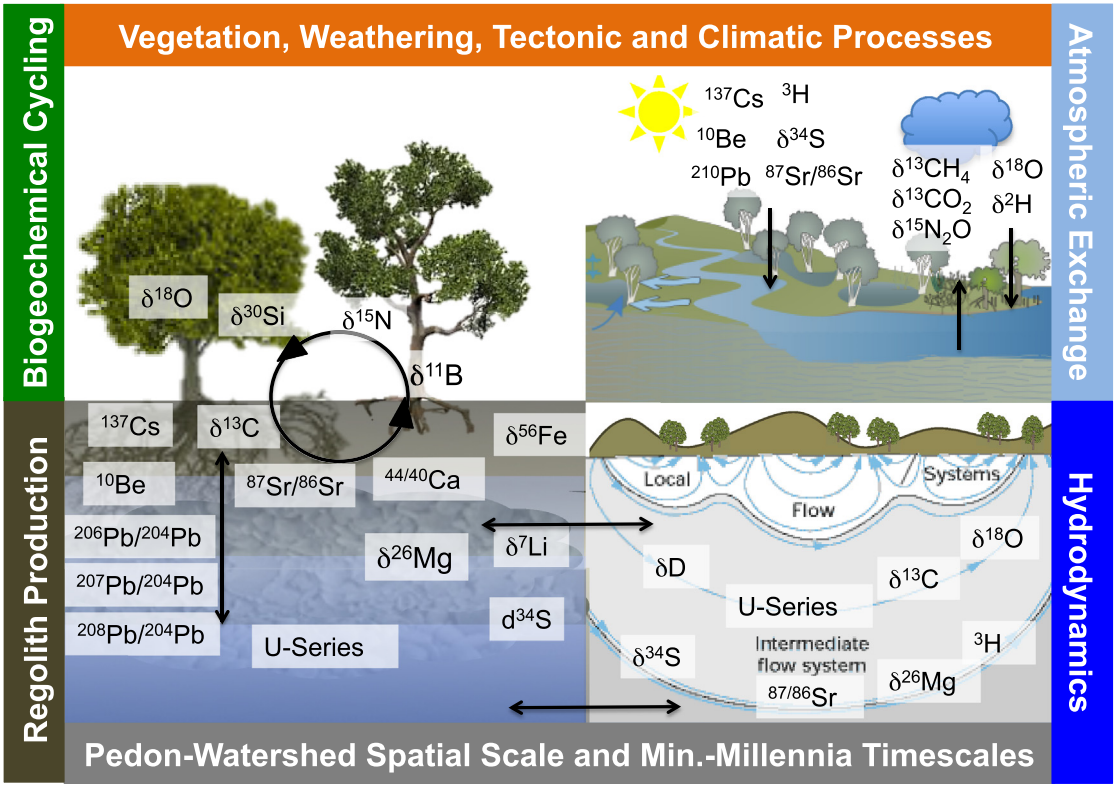

Fig. 1. Multiple isotope systems can be analyzed on the exact same samples to elucidate CZ processes.

Please cite this article as: Sullivan, P.L., et al., CZ-tope at Susquehanna Shale Hills CZO: Synthesizing multiple isotope proxies to elucidate Critical Zone processes across timescal..., Chem. Geol. (2016), http://dx.doi.org/10.1016/j.chemgeo.2016.05.012

Table 1
Summary of common isotope systems used to investigate Critical Zone processes, rates and fluxes.

Element	Isotope	Medium	How the ratio is changed	What they record (source, rate, processes)
H	^{2}H, ^{1}H	Water, gas	Fractionation between phases, mixing	• Mixing of different water pools (Kendall and Caldwell, 1998) • Evaporation and condensation processes • See review of Kendall and Doktor (2003)
	^{3}H	Water, gas	Cosmogenic production, radioactive decay, mixing	• Tracer for young (<65 years) water • Mixing of young and old groundwater • Mean transit time of groundwater • See Schlosser et al. (1988)
Li	^{6}Li, ^{7}Li	Soil, water	Chemical transformation	• Dissolution of mineral • Adsorption on mineral surface (Pistiner and Henderson, 2003) • Formation of secondary minerals and oxides (Huh et al., 1998; Dellinger et al., 2015) • Groundwater flow pathways • For review see Burton and Vigier, 2012; Schmitt et al., 2012
Be	^{7}Be, ^{10}Be	Soil	Cosmic rays	• Regolith residence time (Pavich et al., 1986) • Mobile regolith flux (McKean et al., 1993) • Regolith production (Heimsath et al., 1997)
B	^{10}B, ^{11}B	Soil, water, vegetation	Chemical transformation, mixing	• Adsorption on mineral surface (Lemarchand et al., 2005, 2007) • Formation of secondary minerals (Spivack et al., 1987; Rose et al., 2000) • Groundwater source (Vengosh et al., 1994; Meredith et al., 2013; Lemarchand and Gaillardet, 2006) • Plant cycling (Cividini et al., 2010) • Mixing of different water pools (Chetelat et al., 2005; Chetelat et al., 2009) • For a review see Schmitt et al. (2012)
C	^{12}C, ^{13}C	Soil, water, gas, vegetation	Chemical transformation	• Soil respiration (Cerling et al., 1991) • Land-air CO_2 exchange (Trumbore, 2000) • Photosynthesis pathways (Vogel, 1993) • Plant water/nitrogen limitation (Billings et al., 2016) • Dissolution of silicate versus carbonate minerals (Jin et al., 2009) • Sources of carbon when mixing of different carbon pools (Karim and Veizer, 2000, Rive et al., 2013)
N	^{14}N, ^{15}N	Soil, water, gas, vegetation	Chemical transformations	• N mineralization rates, N loss rates, N inputs, plant N species preferences and allocation patterns (Billen et al., 2007; Sebilo et al., 2013) • Different input sources • Plant N cycling • Microbial discrimination • See Michener and Lajtha (2008)
O	^{18}O, ^{16}O	Water, gas	Fractionation between phases	• Source provenance • Mixing of different water pools (Kendall and Caldwell, 1998) • Evaporation, transpiration, and condensation processes • See review (Kendall and Doktor, 2003)
Mg	^{26}Mg, ^{25}Mg, ^{24}Mg	Water, soil, vegetation	Chemical transformation	• Formation of secondary minerals (Galy et al., 2002; Tipper et al., 2006) • Dissolution of primary minerals (Galy et al., 2002; Tipper et al., 2006) • Mixing of different water pools (Tipper et al., 2006) • Plant uptake • For an overview see Schmitt et al. (2012)
Si	^{28}Si, ^{29}Si, ^{30}Si,	Soil, water, vegetation	Chemical transformation	• Secondary mineral formation (Ziegler et al., 2005) • Plant uptake (Delvigne et al., 2009) • Biomineralization (De La Rocha et al., 1997) • For a review see Opfergelt and Delmelle (2012)
S	^{32}S, ^{33}S, ^{34}S	Soil, water, gas	Fractionation between phases, chemical transformation	• Redox reactions (Strauss, 1999) • Sources of S when mixing of different S pools (Clark and Fritz, 1997)
Ca	^{44}Ca, ^{42}Ca, ^{40}Ca	Soil, water, vegetation	Chemical transformation	• Plant uptake (Page et al., 2008) • Source provenance (Farkas et al., 2011) • For a review see Fantle and Tipper (2014), Schmitt et al. (2012)
Fe	^{54}Fe, ^{56}Fe, ^{57}Fe, ^{58}Fe	Soil, water, vegetation	Chemical transformation	• Abiotic and biotic mediated redox reactions (Melton et al., 2014) • Dissolution processes (Bergquist and Boyle, 2006) • Plant uptake (Guelke and Von Blanckenburg, 2007)
Ge, Si	Ge/Si	Soil, water, vegetation	Chemical transformation	• Similar to Si isotope ratios • Distinguishing between secondary clay formation and plant uptake • Mineral-water fractionation (Kurtz et al., 2002) • Secondary mineral formation (Evans and Derry, 2002) • Plant uptake (Derry et al., 2005)
Sr	^{87}Sr, ^{86}Sr	Soil, water, vegetation	radiogenic production, mixing	• Mixing processes (Kennedy et al., 1998) • Source provenance (Blum et al., 2002) • Atmospheric deposition (Graustein and Armstrong, 1983)
Cs	^{137}Cs	Soil, sediment	Radioactive decay	• Soil erosion and deposition (Matisoff and Whiting, 2011; Poreba, 2006)
Pb	^{206}Pb, ^{207}Pb, ^{208}Pb	Soil	Radiogenic Production/Decay	• Mixing of different particle sources (Reuer and Weiss, 2002) • Anthropogenic contamination (Roy and Négrel, 2001)
U-Series	^{238}U, ^{234}U, ^{230}Th	Soil	Radiogenic Production/Decay	• Rate of chemical weathering and soil formation (Chabaux et al., 2008)

unweathered bedrock, or protolith, consists largely of quartz and the clay minerals illite and chlorite, with plagioclase feldspar in trace amounts. In addition, pyrite and carbonate minerals (ankerite and calcite) are present especially at depth (Jin et al., 2010).

SSHCZO is characterized by a pronounced topographic asymmetry, with steeper north-facing than south-facing hillslopes (20° and 15°, respectively). These north-facing hillslopes are also mantled with thicker and more variable regolith than south-facing hillslopes (West et al.,

Please cite this article as: Sullivan, P.L., et al., CZ-tope at Susquehanna Shale Hills CZO: Synthesizing multiple isotope proxies to elucidate Critical Zone processes across timescal..., Chem. Geol. (2016), http://dx.doi.org/10.1016/j.chemgeo.2016.05.012

Table 2
Candidate sites for employing the CZ-tope approach.

	Susquehanna Shale Hill (PA, USA)	Strengbach (France)	Guadalupe (France)	Rio Icacos (Puerto Rico, USA)	Damma Glacier (Switzerland)	Hawaii (USA)
Site characteristics						
Lithology	Shale	Granite	Andesite	Quartz diorite	Granite	Pumice, volcanic, basalt
MAT (°C)	10	6	23	22	2.2	16
MAP (mm)	1070	1400	1800– > 8000	4235	2300	2500
CZ processes from seconds to decades						
Plant-water-nutrient uptake	H, O (Gaines et al., 2015)				O (Tamburini et al., 2012)	
	Ca, Ge, Sr. Si (Meek et al., 2016)	Ca (Cenki-Tok et al., 2009)	Si (Opfergelt et al., 2012b)	Ca, Ge, Sr. Si (Pett-Ridge et al., 2009a)	Sr (de Souza et al., 2010) Ca (Hindshaw et al., 2013)	Ca, Sr Ba (Kennedy et al., 1998; Wiegand et al., 2005; Bullen and Chadwick, 2015)
		B (Cividini et al., 2010)			C (Guelland et al., 2013) Fe (Kiczka et al., 2010)	
Hydrodynamics/hydrologic cycle	H, O, (Jin et al., 2011; Thomas et al., 2013) H (Sullivan et al., 2016)	H, O (Ladouche et al., 2001; Viville et al., 2006) U-Series (Riotte and Chabaux, 1999; Pierret et al., 2014)		H, O (Scholl et al., 2015)		
	S, C (Jin et al., 2014)	Sr (Aubert et al., 2002; Pierret et al., 2014)	C (Lloret et al., 2011)	Ge, Si (Kurtz et al., 2011)		
CZ processes from decades to centuries						
Anthropogenic inputs	Pb (Ma et al., 2014), ^{137}CS (this issue)					Pb (Monastra et al., 2004)
CZ processes from centuries to millennia						
Weathering	Mg (Ma et al., 2015) Fe (Yesavage et al., 2012) C (Jin et al., 2014; Brantley et al., 2013)		Mg (Opfergelt et al., 2012a)		Mg (Tipper et al., 2012) Fe (Kiczka et al., 2011)	Fe (Thompson et al., 2007)
	B (Noireaux et al., 2014)	B (Cividini et al., 2010)	B (Louvat et al., 2011)			
	Si, Ca, Sr (Meek et al., 2016)	Li (Lemarchand et al., 2010)		Si (Ziegler et al., 2005)	Ca (Hindshaw et al., 2011)	Li (Huh et al., 2004; Pistiner and Henderson, 2003)
		Sr (Probst et al., 2000) Nd (Aubert et al., 2001)		Sr, Nd (Pett-Ridge et al., 2009b)	Sr (de Souza et al., 2010)	Sr (Stewart et al., 2001)
Erosion/soil formation	Be (West et al., 2013; West et al., 2014)					
	U-series (Ma et al., 2010, 2013)		U-series (Ma et al., 2012)	U-series (Chabaux et al., 2013; Dosseto et al., 2012)		U-series (Pett-Ridge et al., 2007)

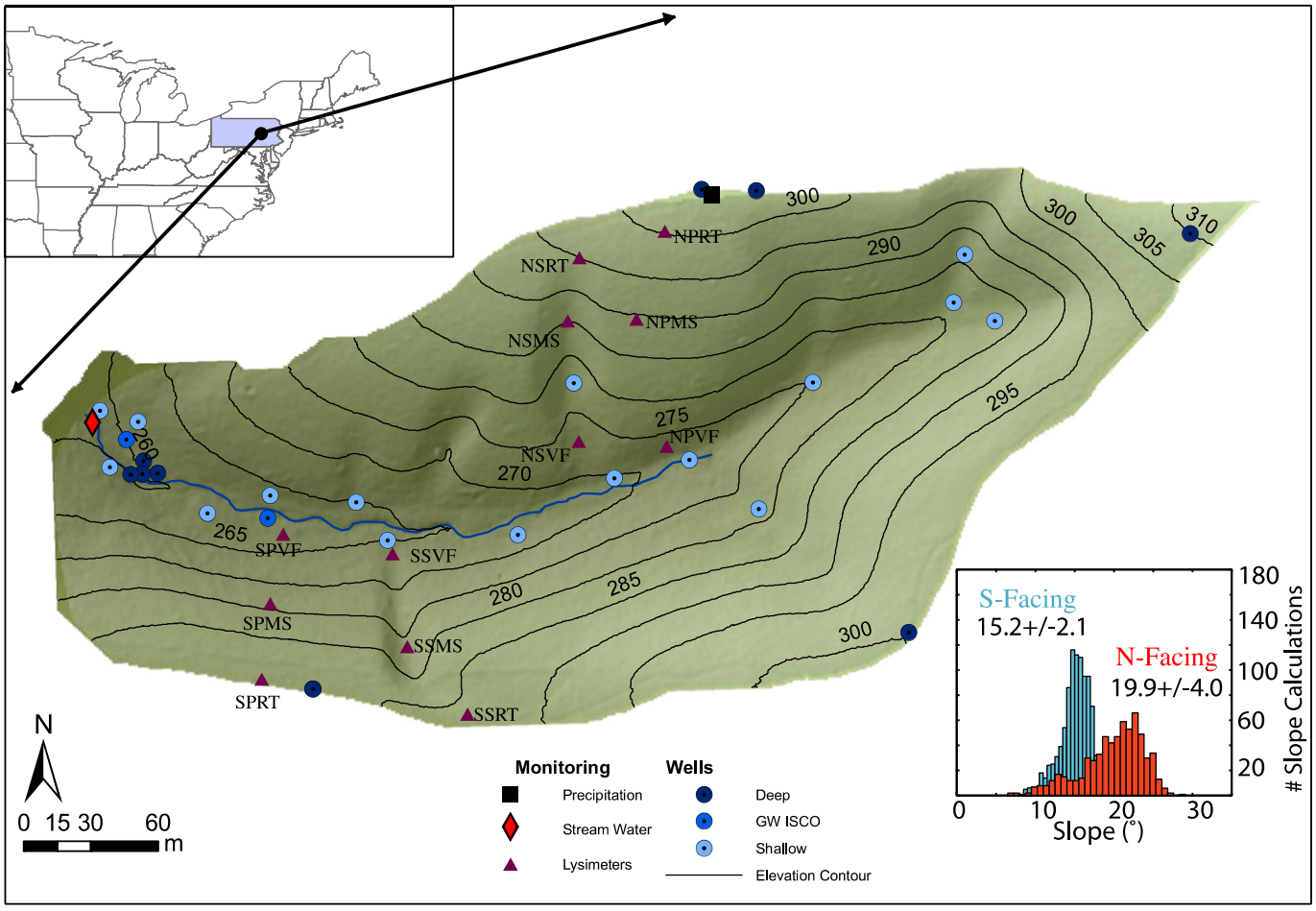

Fig. 2. SSHCZO (Pennsylvania, U.S.A.; top left) is characterized by steeper north-facing hillslopes as compared to south-facing hillslopes (histogram lower right). The multiple isotope systems measured on the exact same soil and rock samples (termed the CZ-tope approach) were collected with installation of soil lysimeters and groundwater wells. There are four transects of nested lysimeters located on the North (N) and South (S) hillslopes; on each respective side, one transect crosses a Planar (P; convex) hillslope, while the other crosses a Swale (S; concave) hillslope. Within each transect there are three nests of lysimeters that stretch from the Ridgetop (RT) to the Midslope (MS) to the Valley Floor (VF).

2014). In general, the morphology of SSHCZO can be characterized by abundant near-planar hillslopes, which are infrequently bisected by hydrologically active swales that experience convergent water and sediment flow. Across the hillslopes, soils generally thicken from the ridge top toward the valley floor with the thicker soils observed in swales and thinner soils present on near-planar slopes (Jin and Brantley, 2011; Lin et al., 2006). In the swales, soils consist of shale colluvium or residuum, including rock fragments. The augerable regolith on the north-facing slopes (which we interpret to be the mobile soil) is underlain by ~1–2 m thick coarse colluvium near the valley floor (West et al., 2013, 2014). The presence and character of this material is consistent with periglacial deposits commonly found in central Pennsylvania (Clarke and Ciolkosz, 1988). At the end of the Pleistocene, SSHCZO resided ~75 km south of the Laurentide Ice sheet and likely experienced periglacial climate conditions; thus, the colluvial material in hillslope swales and under the valley floor are attributed to periglacial processes during this period. Presently, the area experiences a humid-temperate climate where the 30-year averages of precipitation and temperature are 107 cm yr^{-1} and 10 °C, respectively (USC00368449 location, NOAA 2007).

The SSHCZO represents an ideal location to apply the CZ-tope approach as the site's lithology is well characterized and it is equipped for quantifying modern hydrometeorological and gas fluxes. Precipitation is measured using an Ott-Pluvio weighing bucket (Hach Company), Laser Precipitation Monitor (LPM, Thesis Clima), snow depth sensor and snow scale. Eddy covariance measurements are made to quantify the energy budget (i.e., evapotranspiration) and fluxes of CO_2. Soil water fluxes can be estimated from distributed soil moisture probes (Decagon Echo2 Probes) across the catchment, while stream water discharge is quantified using a double V-notch weir located at the outlet and a rating curve established by Nutter (1964). Finally, numerous soil tension lysimeters (depths ranging 10–350 cm) and groundwater wells (depths ranging 2–50 m) provide access to the subsurface solute chemistry. Portions of these data were used to develop and test the Penn State Integrated Hydrologic Model (PIHM; Qu and Duffy, 2007), which has recently been coupled to a land surface model (Flux-PIHM; Shi et al., 2013) for use at the site.

3. Nested reaction fronts develop in the subsurface over millennia

During water-rock interactions, primary minerals transform into secondary phases, solutes are generated, and the bedrock or parent sediments are converted to soils, which can be mobilized and transported downslope (Anderson et al., 2004; Brantley and White, 2009; Chadwick et al., 1990; Jin et al., 2010; Stallard, 1992; White et al., 2005). Thus, the mineral dissolution kinetics have important implications for the development of subsurface reaction fronts, and landscape evolution (e.g., Anderson et al., 2007; Brantley et al., 2007; Ma et al., 2013). Reaction fronts are defined here as the depth intervals across which mineral abundances significantly change within a weathering profile such that above the reaction front the relative mineral abundance is either low or fully depleted, while below the reaction front the relative mineral abundance is high and generally approaches values similar to that of the protolith. The depth sequence of nested reaction

Please cite this article as: Sullivan, P.L., et al., CZ-tope at Susquehanna Shale Hills CZO: Synthesizing multiple isotope proxies to elucidate Critical Zone processes across timescal..., Chem. Geol. (2016), http://dx.doi.org/10.1016/j.chemgeo.2016.05.012

Table 3
Additional site characterization information for the SSHCZO.

SSHCZO pools	Description
Vegetation community (Thomas et al., 2013; Gaines et al., 2015)	• Forest last harvested in the 1930s • Dominated by *Quercus* (Oaks), *Carya* (Hickory) and *Acer* (Maples) • *Tsuga* (Fir) and *Pinus* (Pine) present in the valley floor
Soil structure (Lin et al., 2006)	• Augerable soils to depths of ~30 cm on ridgetops and 397 cm in valley floor • Soils series abundance: Weikert (Planar Hillslopes) > Earnest (Valley) > Rushtown (Swales) > Berks (Swale-Planar transition) > Blairton • Soil texture: Silt loam, Silty clay loam, Loam and Sandy loam
Soil properties (Lin et al., 2006)	• Porosity: 0.84 (surface) to 0.34 (>1 m deep) • Saturated Hydraulic Conductivity: Vertical 13.589 cm min^{-1} (surface) to 0.007 cm min^{-1} (>1 m deep); Horizontal 4.637 cm min^{-1} (surface) to 0.002 cm min^{-1} (>1 m deep)
Soil chemistry (Jin et al., 2010)	• Soil pH: 3.5–5.0 (increasing with depth) • Cation Exchange Capacity: 34.3–88.9 meq/kg increasing downslope and highest in parent material
Soil carbon and nitrogen (Andrews et al., 2011)	• Soil Organic Carbon: 0.25–2.75% (highest concentration in surface soil) • Soil carbonate content: Depleted
Microbial community (Yesavage et al., 2012)	• Microbial cell counts were highest at the surface and decreased with depth • Heterotrophic cell counts varied with depth and were elevated near soil horizon interfaces • Fe-related bacteria were present near the surface along the entire hillslope as well as present at bedrock-regolith interface • Fe-reducing organisms were present but not active in these zones

fronts in a weathering profile differs because the reactivity and abundances of different minerals for a given type of bedrock differ (Brantley and White, 2009). For example, rigorous chemical and mineralogical characterizations from nine boreholes (five on the ridgetop reaching 7.5–30 m deep and four in the valley floor reaching 15 m deep) in the regolith developed on the Silurian Rose Hill (gray shale) formation at SSHCZO have demonstrated that the deepest reaction in the subsurface is pyrite oxidative dissolution, followed or accompanied by chlorite oxidation, carbonate dissolution, and then at much shallower depths, plagioclase and then illite dissolution (Fig. 3; Brantley et al., 2013; Jin et al., 2010; Sullivan et al., 2016).

Shales are fine-grained sedimentary units whose matrix is characterized by low permeability. However, shales are also characterized by fractures at all scales that enhance permeability. For example, optical televiewer data demonstrate that bedding- parallel fractures are common throughout the SSHCZO in the Rose Hill Shale. Hydraulic conductivity tests (pumping and permeameter) and tracer studies indicate that fractures have opened to provide higher permeability, in the upper 6 m throughout the catchment (Brantley et al., 2013; Jin et al., 2011; Kurtz et al., 2011; Sullivan et al., 2016). In addition to these fractures that have been attributed largely to freeze-thaw mechanisms, other physical, chemical and biological processes also affect porosity and permeability (Jin et al., 2011). For example, the dissolution reaction fronts mark the loss of soluble elements by chemical weathering (acid-base and redox reactions), which is likely marked by a decrease in bulk density and increase in porosity (Navarre-Sitchler et al., 2015). Thus, reaction fronts can be used in part to infer the depth to which acids (CO_2, sulfuric acid, nitric acid, and organic acids) and dissolved oxygen infiltrate in the subsurface (Brantley et al., 2013) as well as yielding information about dominant subsurface flow paths. At the SSHCZO, the depth of augerable (mobile) regolith is consistent with the boundary of the illite reaction front, while the plagioclase reaction front coincides with the depth of the highly fractured rock (gray zone ~6 m deep, Fig. 3). Under the ridges, carbonate, chlorite, and pyrite reaction fronts are roughly co-located with the average groundwater table position. Below, we synthesize the isotopic evidence (H/O, ^{3}H, Sr, S, and C) as it relates to the development and evolution of nested reaction fronts across SSHCZO (ridge top versus valley floor; Fig. 3) and their potential role in the development of subsurface flow paths (Jin et al., 2014; Meek et al., 2016; Sullivan et al., 2016; Thomas et al., 2013).

3.1. Hydrogen and oxygen isotopes

In general, the depth where illite begins to react is co-located with the depth of refusal of augerable soils. This soil, also considered the mobile soil along the hillslope, contains chlorite and its reaction products, vermiculite (Jin et al., 2010). These soils are characterized by layers with contrasting permeability that foster shallow (<150 cm deep) preferential flow paths (Lin and Zhou, 2008; Jin et al., 2011; Thomas et al., 2013). H/O isotopes from four transects of nested hillslope lysimeters, nests located at the ridgetop (10–30 cm deep), midslope (10–340 cm deep) and valley floor (10–340 cm deep), and shallow groundwater wells (<4 m deep) provide evidence of heterogeneity in subsurface water flow at pedon and watershed scales (Thomas et al., 2013). Within the first 1.0 m of ground surface large, variations in the observed soil water isotopic composition were interpreted as high hydraulic conductivity and fast water fluxes, while depths and soils that yielded water with small temporal variability in H/O isotopic composition were interpreted as areas of low hydraulic conductivity and reduced water fluxes (Fig. 3). At depths >1.5 m, soil water isotopic variations attenuated and soil water values were equivalent to those observed in groundwater.

H/O isotopic evidence suggests that water, not lost to evaporation, infiltrates in to subsurface layers which become water-saturated, and then moves as interflow along zones of contrasting permeability within 6 m of the surface, eventually recharging the stream (Thomas et al., 2013; Sullivan et al., 2016). Specifically, the highly fractured rock layer (gray, Fig. 3), the base of which is roughly co-located with the position of the plagioclase reaction front, may represent a second meaningful preferential flow zone. This conceptual model is consistent with fairly young water as estimated using a piston-flow model to interpret concentrations of tritium (^{3}H), a radioactive isotope with a half-life ~12.3 years (Sullivan et al., 2016). Measurements of ^{3}H coupled with dissolved oxygen and SF_6, suggest that in the valley floor, interflow water penetrates well below the water table and mixes with old (apparent groundwater age of ~30 yr), oxygen-poor water (Sullivan et al., 2016). Bulk geochemical analyses and scanning electron microscope (SEM) images from boreholes revealed the oxidative dissolution of both pyrite and chlorite below the channel, and were interpreted to result from such seasonal mixing of subsurface waters. Specifically, it has been inferred that young oxygen-charged shallow groundwater, recharged from hillslope interflow, directs relatively fast-flowing water toward the stream during wet periods (November – May). In contrast, older, oxygen-poor, more slow-flowing groundwater follows the average flow paths of the regional water system during dry periods. Sullivan et al. (2016) argues that mixing of water from fast and slow flow paths governs the depth of pyrite oxidation under the channel. They further postulate that this pyrite oxidation promotes channel incision as it enhances porosity and weakens the rock under the channel. This incision allows drainage of equilibrated groundwater from the ridgetops, which in turn allows bedrock to weather higher in the watershed (Fig. 3). Chlorite oxidative dissolution was not invoked by Sullivan et al. (2016) to regulate the rate of channel incision as the loss of dissolved Mg at depth was not visibly consistent with porosity development (using SEM), such as in the case of rock cracking by biotite oxidation (Navarre-Sitchler et al., 2015).

Please cite this article as: Sullivan, P.L., et al., CZ-tope at Susquehanna Shale Hills CZO: Synthesizing multiple isotope proxies to elucidate Critical Zone processes across timescal..., Chem. Geol. (2016), http://dx.doi.org/10.1016/j.chemgeo.2016.05.012

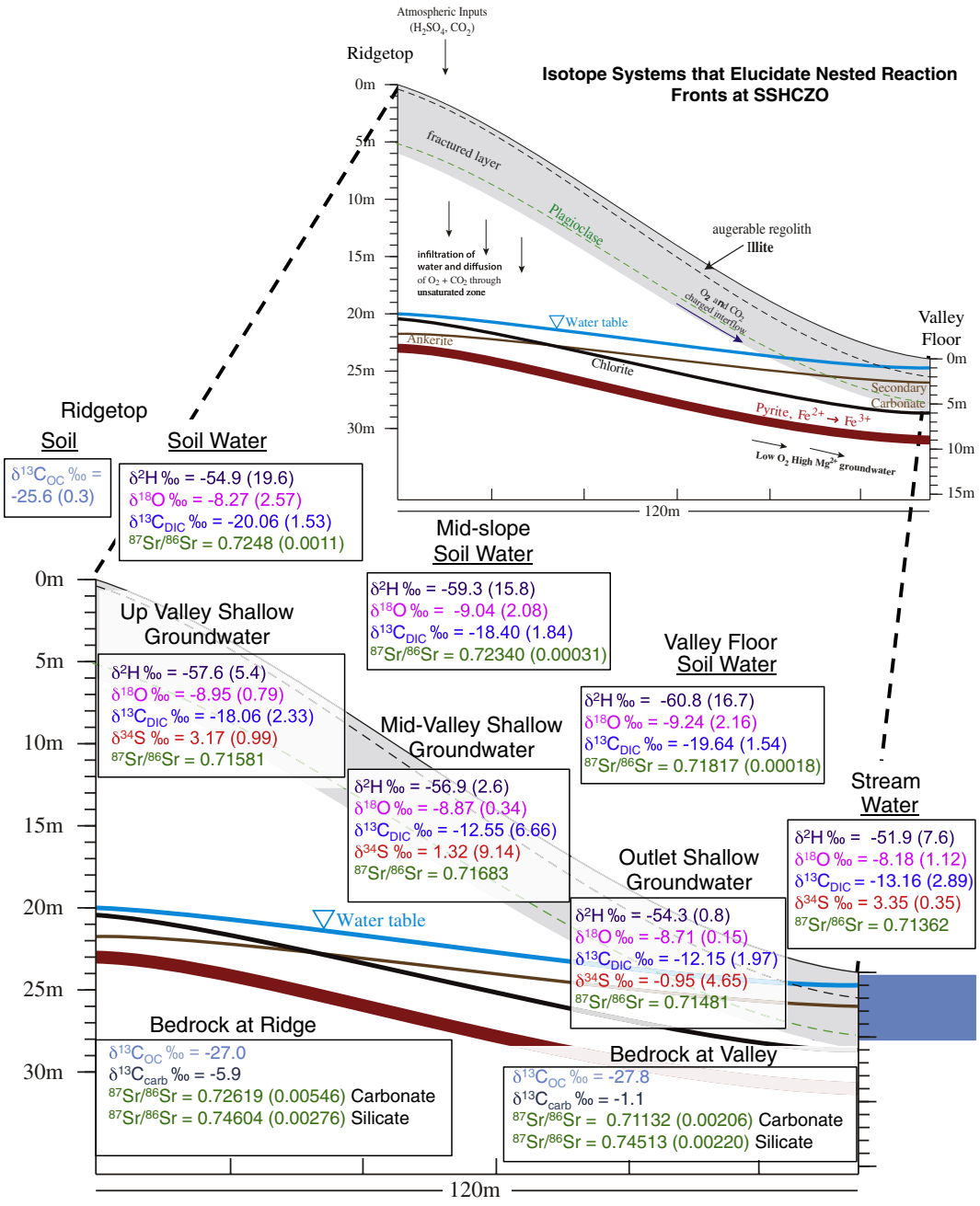

Fig. 3. Top: Nests of reaction fronts were inferred from elemental and mineral abundance analyses on borehole material extracted from nine sites at SSHCZO (figure augmented from Brantley et al., 2013). From deep to shallow we observe oxidative dissolution of pyrite and chlorite, and carbonate, plagioclase and illite dissolution, which were hypothesized to develop in the subsurface due to infiltration of CO_2 and O_2 charged waters. Bottom: The isotopic average (and standard deviation) of $\delta^{13}C$ (blue), $^{87}Sr/^{86}Sr$ (green), and $\delta^{34}S$ (red) from the regolith, bedrock and water, together with δ^2H (purple) and $\delta^{18}O$ (pink) values from various water pools (soil water, stream water and groundwater) support this hypothesis and add that subsurface flow paths govern the advancement of these nested reaction fronts in the CZ over millennia. (For interpretation of the references to color in this figure legend, the reader is referred to the web version of this article.)

3.2. Strontium isotopes

Strontium concentrations and isotope ratios further define multiple flow paths and rock-water interactions at SSHCZO. Soil water Sr (and by inference Ca) at the ridge top and mid-slope positions, documents that shallow soil water contains a mixture of Sr derived from weathered shale and atmospheric deposition (Meek et al., 2016). The observed decrease in $^{87}Sr/^{86}Sr$ from soil pore waters and exchangeable cations over the upper 50 cm indicates soil water is dominated by inputs of comparably less radiogenic atmospheric sources (e.g., precipitation and dry deposition). The valley floor soil water is much less radiogenic, and is influenced by the dissolution of diagenetic calcite, which occurs at shallow depths under the valley (Brantley et al., 2013). A second, somewhat more radiogenic carbonate component is present in ankeritic carbonates at depth (~25 m deep) as measured under the ridgetops. Ankeritic carbonates do not appear to be a major contributor to the stream Sr mass balance as stream water Sr isotopes at the headwater maintain a signature of soil water while those at the outlet approach the less radiogenic shallow groundwater produced by calcite dissolution. In other words, shallow interflow is dominated by infiltrating meteoric waters, which interact with shale along the hillslope and shallow calcite near the valley floor and support the majority of stream flow (evidenced by

Please cite this article as: Sullivan, P.L., et al., CZ-tope at Susquehanna Shale Hills CZO: Synthesizing multiple isotope proxies to elucidate Critical Zone processes across timescal..., Chem. Geol. (2016), http://dx.doi.org/10.1016/j.chemgeo.2016.05.012

stream water $^{87}Sr/^{86}Sr$ values that closely mirrored the calcite signature of the valley floor bedrock and shallow groundwater compositions; Fig. 3), while deep flow paths that interact with the deeper ankerite do not provide significant Sr inputs to the stream.

3.3. Sulfur isotopes

As SSHCZO is located in the zone of the lowest pH rain in the U.S.A., it has been enriched by high concentrations of sulfate and protons by acidic wet deposition (Alewell et al., 2000; Wadleigh et al., 1994). Even though the acidity of rainfall has been significantly reduced through the 1970 Clean Air Act in the U.S.A., the legacy of acid rain has been shown to be long-lasting in the northeastern states (Likens et al., 2002). Furthermore, the pH of the rain in central PA is still often <4 (National Atmospheric Deposition Program). Mass balance and S isotope approaches currently demonstrate that sulfate derived from wet deposition is the major source of dissolved sulfate to the SSHCZO first-order stream (Jin et al., 2014). Only in several shallow groundwater wells did oxidative dissolution of pyrite release sulfuric acids and lead to $\delta^{34}S_{SO4}$ values similar to that of the pyrite in Rose Hill shale. Sulfur isotope data thus documents that most of the S in the stream derives from acid rain (enriched S values). Nonetheless, the pyrite is highly reactive and is releasing isotopically depleted S (Fig. 3).

3.4. Carbon isotopes

Perhaps the most important source of acidity for weathering is carbonic acid. Systematic studies (Jin et al., 2014) on C isotopes at SSHCZO clearly identified biogenic CO_2 as the dominant source of dissolved inorganic carbon (DIC) in soil waters. DIC is produced during weathering of clays and minor feldspar. When soil water moves deep and recharges to the shallow groundwater in the catchment, that water encounters and dissolves carbonate (ankerite or calcite). The DIC produced from carbonate dissolution derives equally from the mineral and from CO_2 in the soil atmosphere. Like the Sr isotopes, the C isotopic signature of ankerite and calcite differed in the bedrock, with calcite enriched in ^{13}C compared to ankerite. In addition, the surface water composition of the carbon isotopes in DIC became increasingly enriched downstream from the headwaters toward the outlet (Jin et al., 2014). These observations combined with Sr concentrations and isotopic ratios (Meek et al., 2016) reinforced the conclusion that the stream water composition is greatly influenced by calcite dissolution near the outlet and that groundwater flow paths that interact with ankerite at depth contribute little to the stream.

Together these multiple isotope systems emphasize that the composition of the SSHCZO stream is dominated by illite and feldspar weathering fluxes generated in the mobile soil and in the upper layer of fractured rock, and by shallow calcite weathering near the valley floor, while ankerite and pyritic weathering fluxes likely leave the catchment in the subsurface as deeper groundwater. Using $^{87}Sr/^{86}Sr$ mass balances and Sr and Ca concentrations in the stream waters, Meek et al. (2016) estimate the propagation of the carbonate front at SSHCZO to be on the order of ~280 m My^{-1}, a value much faster than estimated by regolith production (~17–45 m My^{-1}; Ma et al., 2010, 2014) or erosion (~10.5–25.6 m My^{-1}; West et al., 2013). This carbonate propagation value likely may not represent a long term steady state value as the depth to carbonate front is only ~23 m deep on the ridges and ~3 m deep in the valley (Fig. 3). Specifically, the Sr—Ca mass balance reflects ground and stream water processes measured over relatively short time scales, while the ^{10}Be and U-series constraints on erosion rate and regolith production integrate over much longer time scales. For example, it is possible that the rapid movement of the carbonate front could be attributed to the input of acid rain over the last hundred years. If the carbonate reaction front is indeed propagating faster than other fronts, then the catchment cannot be considered to be in steady state.

4. Freeze-thaw is the dominant soil creep mechanism

Hillslope evolution occurs as a competition between the upward flux of bedrock as it weathers and transforms into regolith, and the downslope flux along hillslopes of regolith materials driven by gravity. Ultimately, the regolith production flux is a function of the rate of uplift, fracturing, and weathering, and includes such processes as frost-cracking, mineral dissolution, and bioturbation (among others). Researchers have shown that the production of regolith is dependent on the regolith thickness, where rates decrease under thicker regolith cover (Heimsath et al., 1997; Ma et al., 2010). The downslope flux of regolith material responds to the hillslope gradient, regolith thickness, and the efficiency of transport processes such as frost-heave, wetting-drying, and bioturbation. In most studies, either the upward or downslope flux is measured, and with the assumption of steady-state, the other flux is inferred.

The SSHCZO is the first watershed where U-series decay chain isotopes (Ma et al., 2010, 2013) and the cosmogenic radionuclide ^{10}Be (West et al., 2013, 2014) have been independently employed to measure the rates of regolith production and transport on the same hillslope, respectively. U-series and ^{10}Be results suggest that regolith production and erosion rates and fluxes are in balance at the ridgetops within the uncertainty (West et al., 2013, Fig. 4). Near the toe of the north-facing hillslope (south slope), Ma et al. (2010, 2013) found that regolith production rates decreased under thickening regolith (Fig. 5). In addition, Ma et al. (2013) reported that regolith production rates on the south-facing slope are generally higher than those of the north-facing slope. Meteoric ^{10}Be concentrations in creeping regolith revealed that downslope fluxes of regolith are equal on both the steep north-facing hillslope mantled with thick regolith and the gentle south-facing slope mantled with thin regolith (West et al., 2014). Intriguingly, this means that both sides of the catchment are eroding at the same rate but that the erosional efficiency of the south-facing side is higher than that on the north-facing side. West et al. (2014) report that regardless of what transport rule is invoked (slope dependent or depth-slope-dependent), regolith transport efficiency is consistently higher on south-facing slopes by a factor of two. Additionally, they found that a transport rule that includes a reduction in disturbance with regolith depth most accurately predicts measured regolith fluxes. These findings indicate that regolith production and transport mechanisms are likely both aspect-dependent and depth-dependent.

One possible mechanism of downslope soil transport is tree throw. However, tree density and functional rooting depths are similar on north- and south-facing slopes at SSHCZO (Gaines et al., 2015) and this makes it difficult to invoke tree throw as the mechanism that explains differences in soil thickness related to aspect. Likewise, no differences have been measured in tree throw density on either side of the catchment (per. Com. Timothy White). In fact, West et al. (2014) argues that the dominant downslope soil transport mechanism is not tree throw, but is freeze-thaw. We therefore argue that differences in regolith thickness are related to differences in production and transport driven by climate perturbation, and most significantly perturbations related to the Last Glacial Maximum (Raab et al., 2007; Schaller et al., 2003). Specifically, aspect-dependent differences in freeze-thaw processes are expected to have resulted in north-facing hillslopes remaining frozen longer (fewer thawing events), reducing the loss of sediment produced on those hillslopes. Conversely, on south-facing slopes, we expect a higher frequency of thawing events to promote removal of material. Since aspect-related differences are minimized near ridge tops, soil production and transport were able to stay in balance at those locations.

Stable isotope ratios ($\delta^{18}O$) measured in natural waters at SSHCZO support aspect-controlled differences in freeze-thaw as a possible mechanism for the evolution of the asymmetric topography at SSHCZO. Thomas et al. (2013) used $\delta^{18}O$ ratios in meteoric, soil, surface, and ground waters to examine the fate of meteoric water entering the

Please cite this article as: Sullivan, P.L., et al., CZ-tope at Susquehanna Shale Hills CZO: Synthesizing multiple isotope proxies to elucidate Critical Zone processes across timescal..., Chem. Geol. (2016), http://dx.doi.org/10.1016/j.chemgeo.2016.05.012

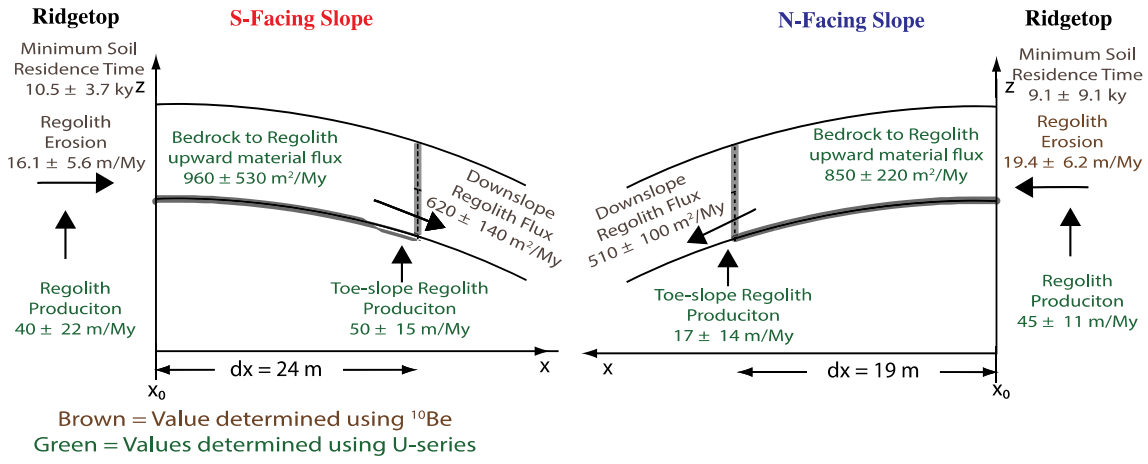

Fig. 4. U-series disequilibrium and meteoric ^{10}Be indicate ridgetop regolith production and erosion rates equate, within error, as do the downslope regolith fluxes, yet toe-slope regolith production values are much greater on the thickly mantled gently sloping S-facing hillslope as compared to the thinly mantled steep N-Facing hillslope (Figure augmented from West et al., 2013).

Shale Hills watershed (Fig. 4). Among their findings, Thomas et al. (2013) measured soil pore waters enriched in $\delta^{18}O$ with respect to meteoric water in the winter months on the north-facing slope of Shale Hills. Soil water $\delta^{18}O$ ratios were similar to meteoric water on the south-facing slope year round. These results suggest that on south-facing slopes, snow pack is quickly melted and meteoric waters infiltrating into soils retain their isotopic composition. However, on north-facing slopes, the slowly melting snow pack enriches water in $\delta^{18}O$, resulting in soil waters enriched in $\delta^{18}O$ values relative to meteoric values.

By combining findings from Ma et al. (2010, 2013); West et al. (2014) and Thomas et al. (2013), we have thus shown a plausible explanation for how microclimatic differences on the north- and south-facing hillslopes at SSHCZO control the frequency of freeze-thaw cycles, with higher frequencies occurring on the sunny south-facing slopes. In turn, this explains the higher erosional efficiency indicated by the high rates of regolith production and thin soils on the sunny slopes. In contrast, on north-facing slopes where regolith remains frozen for more of the year, regolith transport efficiency is interpreted to be lower, perhaps driving lower regolith production rates and less soil thickening. The combination of these studies suggests that the asymmetry observed at SSHCZO has evolved over millennial or longer timescales as a result of aspect-dependent freeze-thaw processes.

5. Significant mass loss occurs as particle transport in the subsurface

Stable Mg, Fe and B isotope ratios can be used to elucidate chemical weathering and erosion processes. To evaluate such critical zone processes, two approaches can be utilized; a soil-focused approach for examining long-timescale weathering, and a water-based approach for understanding short-timescale weathering. Using sampled waters, the general approach is to constrain the isotopic mass balance for any given isotope system under the steady-state assumption. This assumption can be justified if the overall system is changing at a slower rate as compared to the elemental residence times in any given pool or compartment (Bouchez et al., 2013). At SSHCZO, soil residence times span multiple millennia and the near balance in ridgetop regolith production and erosion rates suggest the steady-state assumption is reasonable. In addition, the water residence times at SSHCZO are estimated to range from annual to multi-decadal (Qu and Duffy, 2007; Thomas et al., 2013; Sullivan et al., 2016) suggesting the water pools fluctuate around steady-state and can be utilized as long as they are sampled over the range in hydrologic conditions. The steady-state assumption is that the input fluxes should equate to the output fluxes (F). Taking into account the isotopic signatures (δX) of each flux component results in an equation such as the following (more details in Bouchez et al., 2013)

$$F_{bedrock} = F_{weathering} + F_{erosion}$$
$$\delta X_{bedrock} F_{bedrock} = \delta X_{weathering} F_{weathering} + \delta X_{erosion} F_{erosion}$$

Ideally, one can assess the chemically weathered component by examining the dissolved load in soil solution, stream water, and groundwater, while the erosion component can be determined by estimating soil, bedload and suspended load fluxes. In such a simplified mass balance, the dissolved load should be the complement of the particulate load for each isotope system. The stream water and soil water are, however, impacted by other sources and processes such as precipitation inputs, vegetation cycling, and leaching from leaves as a result of throughfall and dust, while the concentration and composition of particles can be influenced by interaction with dust and organic matter.

At SSHCZO, watershed isotopic mass balances have been fully evaluated using $\delta^{26}Mg$ (Ma et al., 2015) and $\delta^{56}Fe$ (Yesavage et al., 2012). For each isotope system, water pools were sampled over two seasons. The pools included soil, stream and groundwater, while solid samples were collected from bedrock, augerable soil and stream sediments. Augerable soil was collected at multiple depths along a planar hillslope and fluxes were calculated using soil production and erosion rates (Ma et al., 2010, 2013; West et al., 2013) and catchment hydrologic measurements. In both instances the researchers concluded that one isotopic pool was missing or underestimated in the mass balance. For example, for $\delta^{26}Mg$, all measured reservoirs (stream water, groundwater, pore water, stream sediments and soils) were less than or equal to the isotopic signature of the bedrock (0.36‰), indicating a missing component with $\delta^{26}Mg$ values >bedrock (Fig. 6). Ma et al. (2015) suggested this missing component might be attributed to Mg uptake by vegetation (Bolou-Bi et al., 2010), the incorporation of lighter Mg into precipitating carbonate minerals, or the retention of lighter Mg on secondary clay minerals. The authors ruled out vegetation cycling as a significant factor as surface soils (0–10 cm) were not significantly depleted in $\delta^{26}Mg$ compared to soils at depth—an expected pattern if bio-recycling introduced a large fractionation (see Ma et al., 2015). In addition, carbonate precipitation is also unlikely as water pools at SSHCZO have consistently been undersaturated with respect to carbonate minerals (Jin et al., 2010; Jin et al., 2014; Sullivan et al., 2016). Thus, the loss of isotopically light fine clay particles was the most likely mechanism, although the timescale and transport mechanism (stream vs. subsurface flow) was not known.

For $\delta^{56}Fe$, increasingly isotopically light Fe signatures of the solid material indicated enhanced weathering downslope (i.e., $\delta^{56}Fe$ bedrock > ridgetop soil > mid-slope soil > toe-slope soil > stream

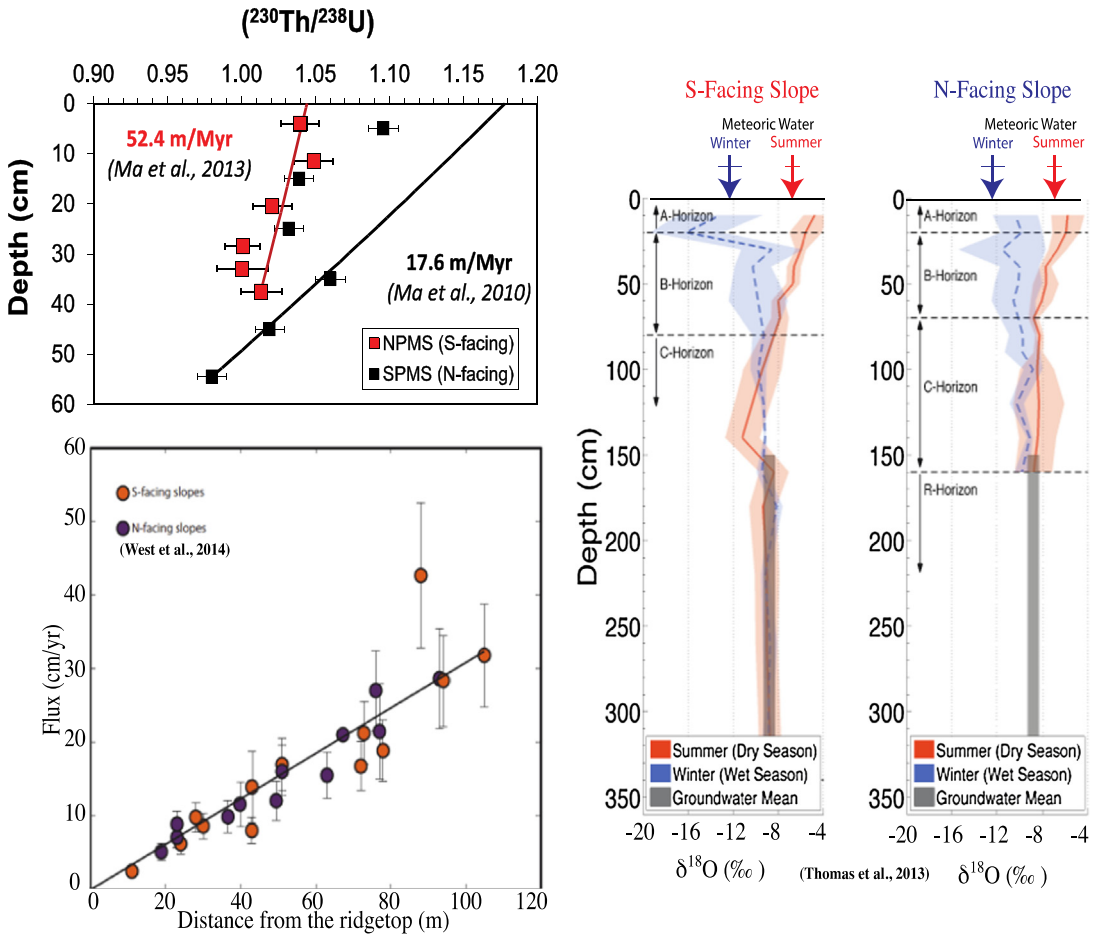

Fig. 5. At SSHCZO regolith production rates based on $^{230}Th/^{238}U$ values were greater on south-facing hillslopes (top left; Ma et al., 2010, 2013) while regolith fluxes, as derived from ^{10}Be measurements, (bottom left; West et al., 2014) were similar on the north facing hillslope (N-facing) and south facing hillslope (S-facing). The asymmetry in production can be explained by aspect controlled freeze thaw events where, S-facing slopes have more thawing events than N-facing slopes, especially under the Last Glacial Maximum climatic conditions. Asymmetric differences in present day winter soil water $\delta^{18}O$ values (left; Thomas et al., 2013) lend support to the hypothesized difference in freeze thaw events. Specifically, during winter soil water on N-facing hillslopes was enriched compared with meteoric inputs (blue arrows), while soil water on the S-facing hillslopes was similar to meteoric water. We can infer from this trend that the snow pack on the S-facing slopes melts quickly and more regularly (i.e., more thawing events), allowing infiltrating meteoric waters to retain their isotopic composition, while snow packs on the N-facing slopes melts slower and less frequently (i.e., fewer thawing events) allowing snow pack to become enriched in $\delta^{18}O$ prior to infiltration.

sediments). Across the hillslope profile soil concentrations of Fe^{2+} were greatest in the bedrock, while Fe^{3+} values were greatest in the soils, with a net loss of Fe^{3+} from the ridgetop and mid-slope positions and a net accumulation of Fe^{3+} at the foot-slope and toe-slope position. In contrast, Fe^{3+} samples in all waters (pore, stream and ground) were very low but demonstrated an increasing trend in concentrations: pore water < stream < groundwater. In all waters, concentrations of Fe^{3+} were nearly double for unfiltered compared to filtered samples. Together these data could be consistent with a sizeable Fe^{3+} loss from the system, perhaps groundwater (see Section 3). One possible mechanism invoked to explain these patterns is fractionation occurring during Fe precipitation but not dissolution, hence isotopically light Fe precipitates in the soils along the flow path and isotopically heavy Fe is lost from the system as micron-sized particles, perhaps in groundwater.

For both Mg and Fe, micron-sized particles — presumably not sampled in lysimeter samples nor in sediments — were invoked to explain the missing pool. The CZ-tope approach of analysis on the same sites and samples has yielded more insight on this missing reservoir. Specifically, Noireaux et al. (2014) analyzed $\delta^{11}B$ from the exact same planar transect soils analyzed for $\delta^{26}Mg$ and $\delta^{56}Fe$, i.e., the ridgetop and valley floor (Fig. 6). The valley floor soil profile had an isotopic signature similar to that of the bedrock and boron losses were attributed to losses of fine particles (clay) that were not isotopically fractionated. Conversely, B concentrations and isotopic values were depleted on the ridgetop, a pattern consistent with mineral dissolution and subsequent adsorption or secondary clay formation.

The loss of particles is consistent with the interpretation of bulk soil geochemical analyses from the ridgetops. A comparison of B/Al and Mg/Al to B/Zr and Mg/Zr, concentrations versus depth in the soil profiles also indicates loss of both solubilized Mg (recorded by Mg/Al) and Al-containing particulates with Mg (recorded by Mg/Zr) (Fig. 6; Noireaux et al., 2014). Together these data suggest that shales lose micron-sized particles that go unrecorded when only filtered water or downhillslope soil creep is considered. Questions still remain as to both when and how these missing fractionated particles were lost from the catchment.

Our current conceptual model is that particles are lost from the soils, transported in the subsurface and exit as subsurface flow and that particle loss was likely greater under peri-glacial conditions when erosion rates were enhanced. Another possible mechanism that could govern the current abundance of isotopic pools at SSHCZO is hydrodynamic sorting during particle transport, similar to observations from large river systems. It could be envisaged that fine grain sizes are exported out of the watershed leaving coarser particles of unweathered bedrock in the streambed sediments. Mg isotopes may support this hypothesis as some particles with a high $\delta^{26}Mg$ were recovered from augering

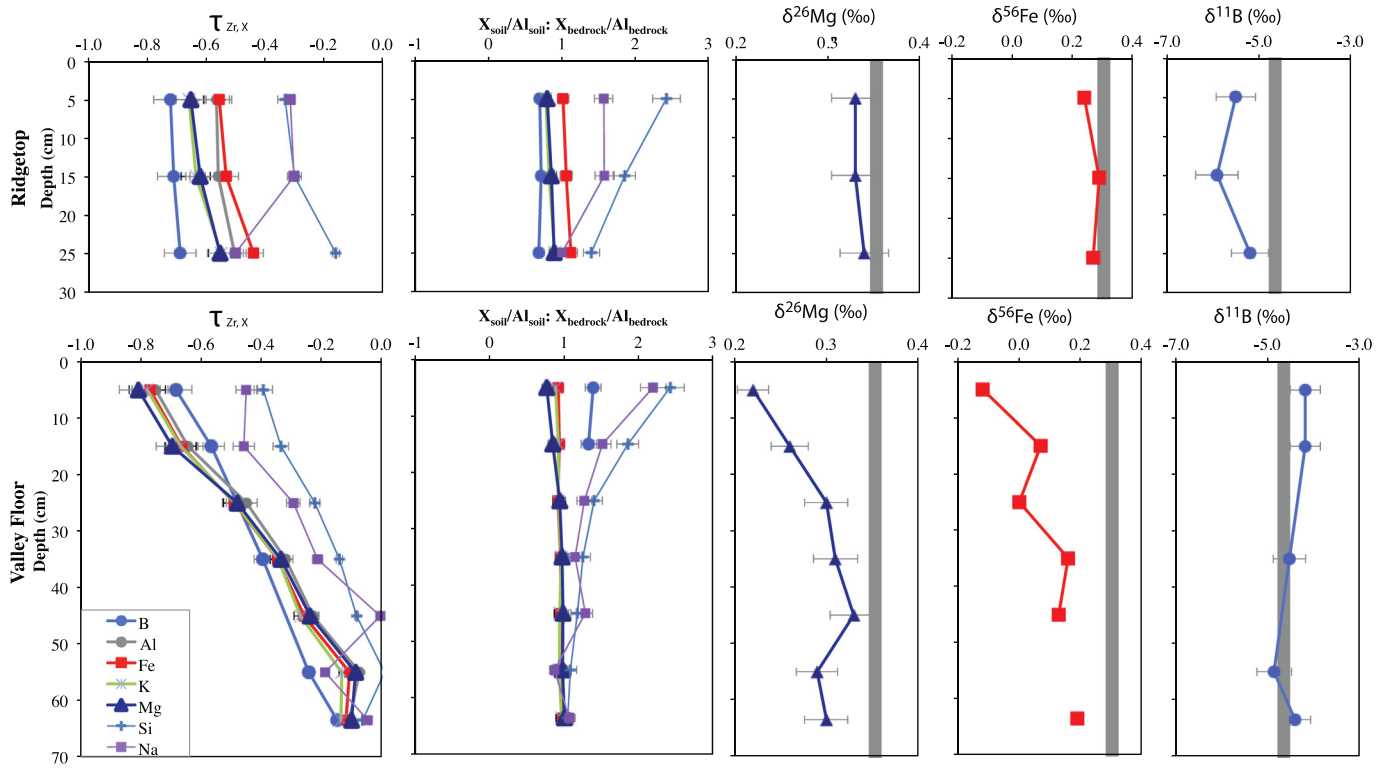

Fig. 6. Depth profiles from the South (S) Planar (P) Ridgetop (top; SPRT) and Valley Floor (Bottom; SPVF): (left) tau values using Zr as immobile element, (left center) soil to bedrock elemental (X) to Al ratios (Jin et al., 2010), (center) δ^{26}Mg (‰; Ma et al., 2015), (right center), δ^{56}Fe (‰; Yesavage et al., 2012), (right) δ^{11}B (‰; Noireaux et al., 2014). Gray vertical bar represents bedrock isotopic composition (center, right center, right).

material beneath the streambed (Ma et al., 2015). This observation could also easily be consistent with movement of particles even at depths under the stream channel too. Recent groundwater observations from the outlet of the SSHCZO suggest that ~4% of the total incoming precipitation is lost as groundwater flow out of the catchment (Sullivan et al., 2016). Thus, if deep groundwater flow carried fine particles, this might represent an unsampled flux.

6. Soils retain the imprint of the industrial revolution

Since the industrial revolution, mining and smelting activities have significantly increased emissions of heavy metals including lead (Pb), copper (Cu), zinc (Zn), cadmium (Cd) and manganese (Mn) to the atmosphere. These metals are subsequently deposited back to Earth's surface, disrupting their natural biogeochemical cycles (Cloquet et al., 2006; Dudka and Adriano, 1997; Galloway et al., 1982; Komarek et al., 2008; Lantzy and Mackenzie, 1979; Nriagu and Pacyna, 1988; Rauch and Pacyna, 2009; Reuer and Weiss, 2002; Taylor et al., 2010).

The SSHCZO has experienced relatively minimal human disturbance in the past century compared to many other watersheds in the more industrialized region of the northeastern United States. However, detailed soil characterizations at Shale Hills have revealed the presence of unusually high levels of Mn, Pb, and Zn in surface soils (Herndon et al., 2011; Kraepiel et al., 2015; Ma et al., 2014). Previous mass balance calculations based on Mn concentrations in bedrock, soil, precipitation, and soil pore water have demonstrated that atmospheric deposition at Shale Hills is the main source of the Mn enrichment. Herndon et al. (2011) hypothesized that the Mn enrichment can be attributed to: 1) iron production in the 19th century in Pennsylvania; 2) upwind modern steel plants and coal-burning power plants; and 3) contributions from recent gasoline combustion. Contributions of Mn from iron ore smelting (from 1850 to 1920) were particularly highlighted as important. Indeed, during the peak of iron production in the mid-1800s, there were approximately 90 operational furnaces and forges in Central Pennsylvania (Eggert, 1994), with several located a few kilometers of SSHCZO. In a recent study, Ma et al. (2014) combined Pb concentrations and Pb isotopic ratios with mass balance and diffusive transport models to show that the dominant source of Pb in soil profiles was likely derived from Pennsylvania coals and or Pb ores used during the iron production period in the local Shale Hills area. However, the timing of the metal deposition event and the possible metal redistribution history was not investigated in the previous studies.

Soil inventories of Cesium-137 (^{137}Cs), a fission product, can be used to interpret recent erosion and deposition that have occurred over the past half-century. In the continental USA, measureable quantities ^{137}Cs were first released in to the atmosphere during atomic weapons testing that began in 1945. Fallout was detectable between approximately 1954 and 1983, with the maximum fallout occurring in 1963 (Matisoff and Whiting, 2011). Central Pennsylvania did not receive fallout from the two large nuclear catastrophes of the past several decades — Chernobyl (1986 — Ukrainie) and Fukushima (2011 — Japan); hence, the location of ^{137}Cs in the soil profile can be used to interpret net erosion or deposition since 1963. We combine new ^{137}Cs profiles at Shale Hills with previous results from a Pb diffusive migration model to further investigate the timing of the metal deposition and the soil erosion or deposition history at Shale Hills.

Again the CZ-tope approach was employed by analyzing the same soil profiles from the south slopes (planar and swale) for bulk chemistry and isotope ratios of ^{206}Pb/^{204}Pb, and inventories of ^{137}Cs. Inventories at SSHCZO show ^{137}Cs peaking very shallow in the profile, within the top decimeter (Fig. 7). The total ^{137}Cs inventory at the south planar midslope (SPMS) profile was 1610 Bq m^{-2}. In the nearby south swale ridgetop (SSRT) and midslope (SSMS) profiles, total inventories were 1180 Bq m^{-2} and 920 Bq m^{-2}, respectively. The U.S. Center for Disease Control estimates 4000–6000 Bq m^{-2} of fallout over the central Pennsylvania area (Matisoff and Whiting, 2011), with the peak in fallout occurring in 1963. Given the half-life of ~30.2 years, this equates to approximately 1200–1900 Bq m^{-2} of ^{137}Cs activity remaining at

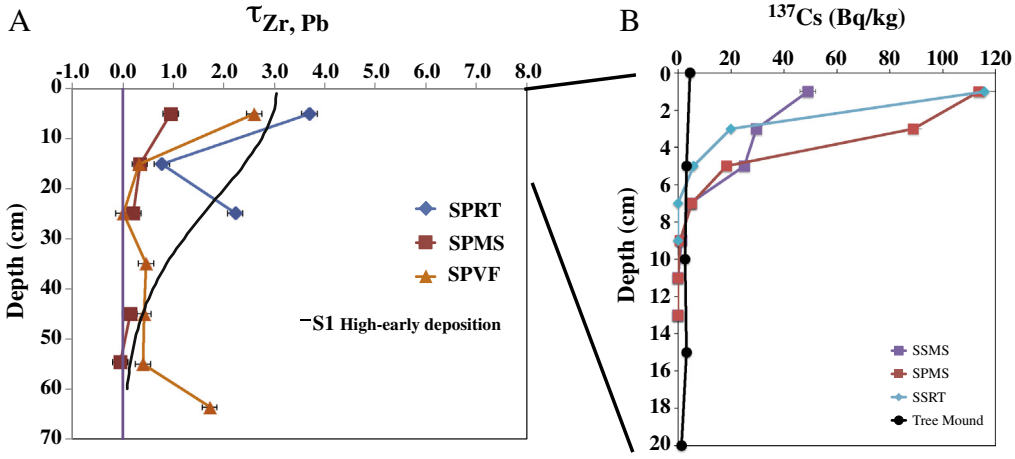

Fig. 7. A. Measured $\tau_{Zr,Pb}$ values in soils are shown for a ridgetop (SPRT; blue), midslope (SPMS; red), and valley floor (SPVF; orange). Pb redistribution in soil profiles is modeled by a diffusive transport model (Drivas et al., 2011). Black solid curve represents a period of continuous high Pb deposition rate (10 mg cm^{-2} yr^{-1}) for 70 years followed by a period of 90-year deposition-free time (Scenario 1: Ma et al., 2014). B. Measured ^{137}Cs values shown for the ridge top (SSRT; blue), two mid-slope positions (SSMS (purple) and SPMS (red)) and a tree mound (black). (For interpretation of the references to color in this figure legend, the reader is referred to the web version of this article.)

reference sites as of our sampling in 2013. The SPMS site inventory is consistent with this range, but the inventories at SSRT and SSMS are too low. Perhaps, the SPMS site has not experienced measurable net erosion or deposition over the past 50 years, while the SSRT and SSMS sites have both experienced net erosion over the past 50 years.

Pb concentrations in SPRT, SPMS, and SPVF profiles were characterized by calculating their mass transfer coefficients ($\tau_{Zr,Pb}$) (Ma et al., 2014). This calculation uses an immobile element (e.g. Zr) to normalize Pb concentrations. Positive $\tau_{Zr,Pb}$ values indicate enrichment of Pb, negative values indicate depletion, and zero indicates no gain nor loss of Pb in the weathered soils with respect to the parent material. Values of the bulk soils in the SPRT, SPMS and SPVF profiles are mostly all positive and increase toward the surface (Fig. 7). Indeed, the surface soils from 0 to 10 cm depth have higher $\tau_{Zr,Pb}$ values (0.96 to 3.71), consistent with Pb enrichments of 96 to 371% compared to the parent material. These profiles thus are characterized as addition profiles (Brantley and White, 2009). For a ridgetop soil, addition cannot come from downslope transport and the source must therefore be atmospheric and/or anthropogenic addition. The deep soil samples (e.g. 20–70 cm depth) in SPRT and SPVF show $\tau_{Zr,Pb} > 0$, documenting Pb addition in the deep soils. Furthermore, Pb isotope ratios at Shale Hills (Ma et al., 2014) have revealed the presence of anthropogenic Pb at depth. This is attributed to the redistribution of Pb within the soil column. For example, chemical dissolution and adsorption/reprecipitation at depth, especially given the acidic surface soil waters (pH ~3–5; Andrews et al., 2011), could enhance Pb mobility after deposition. In addition, Pb deposited on the soil surface likely mixes downward in the soil column over time due to physical mixing (e.g., freeze-thaw), bioturbation, and adsorption/desorption (e.g., He and Walling, 1997; Kaste et al., 2007; Drivas et al., 2011).

The ^{137}Cs layer occurs at shallower depth than the Pb-enriched layer in the SPRT profile, indicating Pb deposition mainly occurred prior to ~1963, and can most likely be attributed to the iron production period in Pennsylvania (1850 to 1920). In addition to the horizon markers, the remaining ^{137}Cs at each location provides an indication of the net erosion or deposition that has taken place since the atomic weapons testing era (c. 1963). For example, erosion occurred at ridge top profiles (e.g. SSRT and SPRT) and removed some Pb from the surface over the past 50 years. For example, areas of known disturbance, such as tree-throw mounds, show this mixing though the ^{137}Cs profile, which is homogeneous and low (details below).

These soil profiles provide documentation of the effect of the industrial revolution on soils — local, patchy accumulation of metals such as Pb and Mn (Herndon et al., 2011; Ma et al., 2014) near the many small metal emitters in industrial areas, as well as some long-term accumulation due to more regional fluxes. Local, patchy contamination likely persists wherever atmospheric deposition from anthropogenic sources occurred into metal-retaining soils since the 1850s. The later addition of ^{137}Cs, c. 1963, provides an event horizon and constrains the timing of metal contamination found beneath ^{137}Cs in the soil profiles to before the mid-twentieth century. At SSHCZO, the Pb deposition rate was constrained to be ~10 μg cm^{-2} yr^{-1} by a mass balance model (Ma et al., 2014). Once deposited at Earth's surface, pollutant metals such as Pb and Cs can persist in contaminated soils over considerable lengths of time, e.g. ~50–200 years. Although the enforcement of strict policies such as the U.S. Clean Air Act (1970) effectively reduced metal emissions to the atmosphere a few decades ago, the metals that had already been deposited into topsoils since the advent of the industrial revolution can stay in the environment for at least a few hundred years. Indeed, Herndon et al. (2011) showed historical datasets and hypothesized that over half of the soils surveyed in Pennsylvania and in many industrialized areas of North America and Europe are enriched in Mn, Pb and Cd.

Beyond soil profiles, these isotopes and metals can provide a timeline for substantial mixing of soil profiles, such as that occurring with tree throw. Profiles remaining relatively undisturbed over the past few decades show an event horizon of ^{137}Cs that represents the soil surface at the time of atmospheric weapons testing (c. 1963) (Fig. 7). In contrast, the tree-mound soil profiles show a relatively constant, low-magnitude tracer profile that documents vertical mixing throughout the profile (Fig. 7). Such a deep and homogeneous profile indicates mixing – accumulation in the mound of the root wad material after tree fall – since ~1963.

Interpreting anthropogenic metal and isotopic markers at SSHCZO allows the dating of horizons within the soils from years to over a century. In comparison, our measurements of ^{10}Be and U-series, which elucidate millennial timescale processes, allow us to decipher how short-term and long-term disturbances influence soil formation. For example, short-term disturbance events (i.e., tree throw) may contribute to the small variations in the ^{137}Cs measurements observed at SSHCZO but when Pb, U-series and ^{10}Be values are analyzed, these short-term events are smoothed out, and freeze-thaw processes over long timescales emerges as the primary driver of soil erosion. In addition, measurements of todays' isotopic fluxes ($\delta^{26}Mg$, $\delta^{56}Fe$, $\delta^{11}B$, $\delta^{2}H$, $\delta^{18}O$), and soil production rates over millennial timescales (U-series and ^{10}Be) point to the fact that erosion during the Last Glacial Maximum occurred at faster rates than we see today, and that the catchment has not yet relaxed back to steady-state for all reservoirs.

Please cite this article as: Sullivan, P.L., et al., CZ-tope at Susquehanna Shale Hills CZO: Synthesizing multiple isotope proxies to elucidate Critical Zone processes across timescal..., Chem. Geol. (2016), http://dx.doi.org/10.1016/j.chemgeo.2016.05.012

7. Oxygen isotope fractionation occurring near clay surfaces reveals vegetation relies on immobile soil water at daily to decadal timescales

The CZ-tope approach can provide a pathway for identifying where plants specifically access water and nutrients in the subsurface. For decades now the isotopic composition of xylem water from trees has been used to identify a tree's water sources (Dawson and Ehleringer, 1991; Ehleringer and Dawson, 1992), and the new use of laser techniques to measure isotopes has fueled the number of tree-source water studies (Evaristo et al., 2015). Interestingly, in many catchments, plant water isotopes do not look like the mobile water sampled by low-tension lysimeters nor do they look like the stream or ground waters in many catchments. Instead in those catchments, the xylem water typically resembles the soil water that can be extracted cryogenically or by centrifugation. This bulk soil water plots off the local meteoric water line (LMWL), and is often interpreted to demonstrate a signal of evaporative water loss. This was first observed by Brooks et al. (2009) at the Andrews Experimental Forest in Western Oregon, and was later named the *two-water world hypothesis* (Goldsmith et al., 2012; McDonnell, 2014). Some have interpreted this to mean that trees largely access a pool of tightly-bound water within the soil matrix that does not significantly contribute to runoff.

Three main lines of evidence demonstrate trees at SSHCZO are yet another example of these two-water worlds (Gaines et al., 2015; Fig. 8): 1) generally trees from this temperate forest rely on soil water at depths of 60 cm or less; 2) soil water extracted using cryodistallation techniques is isotopically distinct from soil water extracted under tension lysimeters; and 3) xylem water exhibits an isotopic signature similar to that of bulk, cryogenically-distilled soil water during the growing season. In other words, trees in this catchment are using shallow soil water (<60 cm) that does not resemble ground water or soil water sampled by lysimeters, but rather resembles bulk soil water that includes tightly bound water. While evaporative factors could be invoked to explain the enrichments at SSHCZO, the fairly high relative humidity (~90%) as indicated by the slope of the SSHCZO LMWL (Thomas et al., 2013) suggests this it is likely not a factor governing the observed fractionation in the xylem water. Given that root water uptake under non-saline conditions does not fractionate oxygen and hydrogen isotopes (Dawson and Ehleringer, 1991; Ehleringer and Dawson, 1992), more mechanistic isotopic studies are needed to examine the factors governing isotopic fractionation in the subsurface.

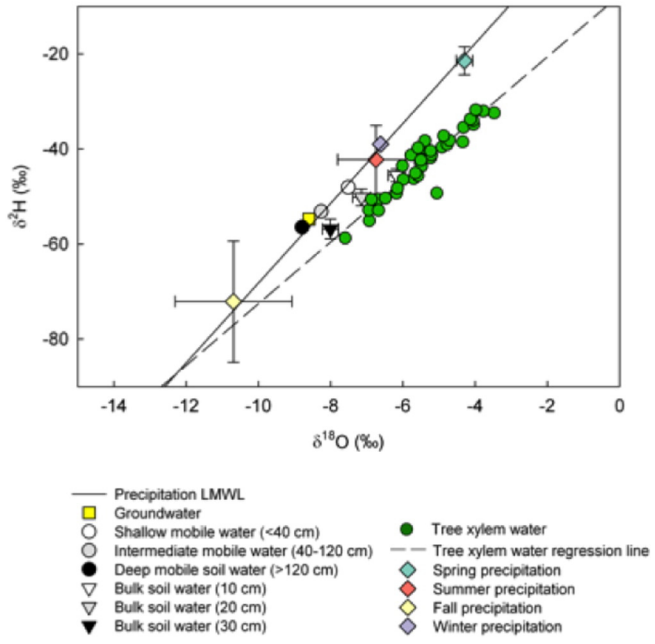

Fig. 8. Xylem water (green circle) collected from trees at SSHCZO as compared to six potential source waters: precipitation (diamonds), bulks soil water (triangles), mobile soil water (circles) and groundwater (square) (data presented in Gaines et al., 2015). Xylem water and bulk soil water fall below the local meteoric water lines (LMWL; $\delta^2H = 8.40 * \delta^{18}O + 15.78$, Thomas et al., 2013; solid line). Xylem water regression line cross $\delta^2H = 6.49 * \delta^{18}O + 15.78$ the LMWL at a δ^2H of −86.1‰ and $\delta^{18}O$ of −12.2‰, which is well below all source waters measured at SSHCZO. (For interpretation of the references to color in this figure legend, the reader is referred to the web version of this article.)

Recently it has been observed that isotopic fractionation of ^{18}O occurs with montomorillonite-associated water as a result of the effect related to electronegative surface charges and cation exchange at the clay surface (Oerter et al., 2014). These authors invoked differences in the structure of the hydration spheres around cations sorbed to clays to explain the differences in isotopic fractionation. A greater fractionation in the water isotopes was hypothesized to occur during hydration around cations with a high charge-to-radius ratio. SSHCZO soils have high clay content (30–65%), porosity of (35–80%) and a cation exchange capacity (34–71 meq/kg), and Al^{3+}, Mg^{2+} and Ca^{2+} dominate the exchange sites (Jin et al., 2010). Given the clays at SSHCZO mainly consist of Mg-rich illite and chlorite with cation exchange sites dominated by high ionic potential cations, it is possible that the Oeter et al., (2014) study, although focused strictly on smectitic clay, could provide an explanation for isotopic fractionation of water at illlite or vermiculate surfaces in the SSHCZO catchment. Fractionation at the clay surfaces is therefore considered a possible mechanism to explain the isotopic distinct differences between mobile and bulk soil water at Shale Hills. This working hypothesis specifically implies that oxygen isotopic fractionation occurs along the surface of illitic and vermiculitic clays, producing a water reservoir which is isotopically enriched in ^{18}O. According to this hypothesis, this reservoir in turn is a primary source of water to the trees.

The behavior of isotopes may allow us to distinguish the true roles of mobile and immobile water in terms of plant ecophysiology and their impact on CZ evolution. Here, we define mobile water as samples from suction cup lysmeters, and immobile water as water associated with the soil exchangeable pool. Specifically, a multiple isotope approach can be used to distinguish the degree to which uptake of water and nutrients (e.g., N, P, Ca, K, Mg, Si) are coupled, and to explore mechanisms of coupling or decoupling. At SSHCZO, Sr isotopes, Ge/Si and Ca/Sr were measured in xylem, lysimeter water, stream and ground waters, the soil exchangeable cations, leaf material from sugar maple (*Acer saccherum*) and red and chestnut oaks (*Quercus rubra*, *Quercus prinus*) and drill core material from two boreholes (Meek et al., 2016). In the upper soils, the ratios of Ca/Sr and Sr isotopes indicated differences in the composition of cations in the mobile domain versus immobile domain. Interestingly Ca/Sr and Sr isotope ratios of the sap water from all species were similar and indicated nutrient inputs from both the mobile and immobile soil domain. Over the growing season, they found that Ca and Si accumulated in canopy leaves, while Ge/Si increased in the soil solution. On net, the authors concluded that the active biological cycling of Ca and Si modified soil solutions and the exchange chemistry of the shallow soils. Given that we know that sorption processes result in the isotopic fractionation of many cations (Table 1), and given our new hypothesis suggesting that clays may act to fractionate water isotopes, future efforts need to focus on differentiating the proportions of sorbed and mobile ions that contribute to the xylem water to elucidate biotic controls on subsurface mobile and immobile domains.

8. Synthesizing isotopic observations

Multiple isotope systems at SSHCZO demonstrate their usefulness for quantifying and comparing CZ fluxes over multiple timescales. New data shows that regolith fluxes are primarily driven by annual freeze thaw cycles operating over millennial timescales, where as the effects of tree throw is less significant in controlling soil creep. Evidence

from isotope proxies over multiple timescales indicates these erosive fluxes were likely greater during the last glacial maximum than what we measure today, and that the fluxes from many CZ pools at SSHCZO are still approaching steady-state conditions. Only at the ridgetops does it appear that the rate of soil production is equal, within error, to the rate of erosion. Chemical weathering in the subsurface results in the development of nested reaction fronts. Part of the "chemical" weathering flux may actually consist of loss of micron-sized particles in the subsurface. Measurements of today's sap water indicates that plants take up both water and nutrients from the mobile and immobile domain located in the upper portion of the soil column, and that the composition of this immobile domain is regulated by exchange on clay surfaces. Finally, human imprint is observed throughout the catchment in the form of relatively high topsoil concentrations of Mn, Pb, and Zn, largely released during the heyday of the Pennsylvania iron industry, but also released from more recent anthropogenic activities. A synthesis of multiple isotopes systems highlights the diverse timescales over which geologic, hydrologic, geochemical, and biological processes operate to drive the evolution of a landscape and the interaction of the compartments within, and the contemporary processes that continue to form it.

9. Developing the CZ-tope approach

This synthesis of the CZ-tope approach at SSHCZO exemplifies the benefits of facilitating multiple isotope analyses on the identical samples as it elucidates CZ processes over multiple timescales at one site. By invoking multiple elemental isotopic signatures on identical samples, we have been able to synthesize a conceptual model for the evolution of SSHCZO and its contemporary dynamics. Such endeavors will be accelerated if Critical Zone Observatories and other similar watershed organizations share samples and data to promote integrative understanding of Earth's surface processes on a multitude of lithologies, in diverse climates and ecosystems. Rather than using the large number of isotopes on different samples and different sites, CZ-tope can focus efforts on a small number of well-understood site for better understanding. Such a CZ-tope approach is feasible, especially given the multitude of observatories that are developing and the proven success in use of isotopes at a few such sites (Table 2). To accelerate such collective progress, data and data sample sharing is required. For example, SSHCZO can share 1) bedrock, regolith and water samples; 2) ancillary data about samples, registered with the Interdisciplinary Earth Data Alliance (IEDA) EarthChem (http://www.earthchem.org/) sponsored by the U.S.A. National Science Foundation; 3) a set of publications hosted online for SSHCZO related to all the isotopic systems discussed in this paper (www.criticalzone.org).

In addition to facilitating the analyses of multiple isotopes on the same samples for sites located around the world, centralizing these isotopic data will also make it possible to advance modeling efforts, including reactive transport models (RTM; Li et al., 2016). Currently, researchers are expanding the use of isotopic (i.e., Ca, S, Sr) modeling to elucidate CZ processes (Druhan et al., 2012, 2013, 2014; Druhan and Maher, 2014) in reactive transport models. For example at SSHCZO, Bao et al. (2016) recently added a RTM module to a hydrologic land surface model (Flux-PIHM) to pave the way for future researchers to integrate these multiple isotope systems into a model domain. Others have incorporated isotopic fractionation into models based on CrunchFLOW (Druhan et al., 2012, 2013, 2014; Druhan and Maher, 2014). Such advances will help to guide future sampling approaches and laboratory experiments. By embracing the CZ-tope approach – a focus on using multiple isotopes on the same samples in the same sites – researchers will solve some of the many mysteries of watershed form, function, and dynamics (such as those proposed by Band et al., 2014; Brantley et al., 2011; Kirchner, 2003; Rempe and Dietrich, 2014).

Acknowledgements

This work was facilitated by NSF Critical Zone Observatory program grants to CJD (EAR 07-25019) and SLB (EAR 12-39285, EAR 13-31726). This research was conducted in Penn State's Stone Valley Forest, which is supported and managed by the Penn State's Forestland Management Office in the College of Agricultural Sciences. We also acknowledge NSF EAR post doc grant (NSF EAR 1144760) for supporting the work of Diana Karwan. We thank the reviewers for thoughtful comments, and for the review by Dr. S Billings.

References

Alewell, C., Mitchell, M.J., Likens, G.E., Krouse, H.R., 2000. Assessing the origin of sulfate deposition at the Hubbard Brook experimental forest. J. Environ. Qual. 29, 759–767.
Anderson, S.P., Blum, J., Brantley, S.L., Chadwick, O., Chorover, J., Derry, L.A., Drever, J.I., Hering, J.G., Kirchner, J.W., Kump, L.R., Richter, D., White, A.F., 2004. Proposed initiative would study Earth's weathering engine. EOS Trans. AGU 85, 265–269.
Anderson, S.P., von Blanckenburg, F., White, A.F.M., 2007. Physical and chemical controls on the critical zone. Elements 3, 315–319.
Andrews, D.M., Lin, H., Zhu, Q., Jin, L., Brantley, S.L., 2011. Hot spots and hot moments of dissolved organic carbon export and soil organic carbon storage in the Shale Hills catchment. Vadose Zone J. 10, 943–954.
Aubert, D., Stille, P., Probst, A., 2001. REE fractionation during granite weathering and removal by waters and suspended loads: Sr and Nd isotopic evidence. Geochim. Cosmochim. Acta 65, 387–406.
Aubert, D., Probst, A., Stille, P., Viville, D., 2002. Evidence of hydrological control of Sr behaviour in stream water (Stengbach catchment, Vosges mountains, France). Appl. Geochem. 17, 285–300.
Band, L.E., McDonnell, J.J., Duncan, J.M., Barros, A., Bejan, A., Burt, T., Dietrich, W.E., Emanuel, R.E., Hwang, T., Katul, G., Kim, Y., McGlynn, B., Miles, B., Porporato, A., Scaife, C., Troch, P.A., 2014. Ecohydrological flow networks in the subsurface. Ecohydrology 7, 1073–1078.
Bao, C., Shi, Y., Sullivan, P.L., Duffy, C., Brantley, S.L., 2016. RT-flux-PIHM: a hydrogeochemical model at the watershed scale. Water Resour. Res.
Bergquist, B.A., Boyle, E.A., 2006. Iron isotopes in the Amazon River system: weathering and transport signatures. Earth Planet. Sci. Lett. 248, 54–68.
Bigalke, M., Weyer, S., Kobza, J., Wilcke, W., 2010. Stable Cu and Zn isotope ratios as tracers of sources and transport of Cu and Zn in contaminated soil. Geochim. Cosmochim. Acta 74, 6801–6813.
Billen, G., Garnier, J., Nemery, J., Sebilo, M., Sferratore, A., Barles, S., Benoit, P., Benoît, M., 2007. A long-term view of nutrient transfers through the seine river continuum. Sci. Total Environ. 375 (1), 80–97.
Billings, S.A., Boone, A.S., Stephen, F.M., 2016. Tree-ring δ13C and δ18O, leaf δ13C and wood and leaf N status demonstrate tree growth strategies and predict susceptibility to disturbance. Tree Physiol. (p.tpw010).
Bolou-Bi, E.B., Poszwa, A., Leyval, C., Vigier, N., 2010. Experimental determination of magnesium isotope fractionation during higher plant growth. Geochim. Cosmochim. Acta 74, 2523–2537.
Blum, J.D., Klaue, A., Nezat, C.A., Driscoll, C.T., Johnson, C.E., Siccama, T.G., Eagar, C., Fahey, T.J., Likens, G.E., 2002. Mycorrhizal weathering of apatite as an important calcium source in base-poor forest ecosystems. Nature 417, 729–731.
Bouchez, J., von Blanckenburg, F., Schuessler, J.A., 2013. Modeling novel stable isotope ratios in the weathering zone. Am. J. Sci. 313, 267–308.
Brantley, S.B., White, A.F., 2009. Approaches to modeling weathered regolith. Rev. Mineral. Geochem. 70, 435–484.
Brantley, S.B., Godhaber, M.B., Ragnarsdottir, K.V., 2007. Crossing disciplines and scales to understand the critical zone. Elements 3, 307–314.
Brantley, S.L., Megonigal, J.P., Scatena, F.N., Balogh-Brunstad, Z., Barnes, R.T., Bruns, M.A., Van Cappellen, P., Dontsova, K., Hartnett, H.E., Hartshorn, A.S., Heimsath, A., Herndon, E., Jin, L., Keller, C.K., Leake, J.R., McDowell, W.H., Meinzer, F.C., Mozdzer, T.J., Petsch, S., Pett-Ridge, J., Pregitzer, K.S., Raymond, P.A., Riebe, C.S., Shumaker, K., Sutton-Grier, A., Walter, R., Yoo, K., 2011. Twelve testable hypotheses on the geobiology of weathering. Geobiology 9, 140–165.
Brantley, S.L., Holleran, M.W., Jin, L., Basilevskaya, E., 2013. Probing deep weathering in the Shale Hills critical zone observatory, Pennsylvania (USA): the hypothesis of nested chemical reaction fronts in the subsurface. Earth Surf. Process. Landf. 38, 1280–1298. http://dx.doi.org/10.1002/esp.3415.
Brooks, J.R., Barnard, H.R., Coulombe, R., McDonnell, J., 2009. Ecological separation of water between trees and streams in a Mediterranean climate. Nat. Geosci. 3, 100–104.
Bullen, T., Chadwick, O., 2015. Evidence for nutrient biolifting in Hawaiian climosequence soils as revealed by alkaline earth metal stable isotope systematics. Procedia Earth Planet. Sci. 13, 312–315.
Burton, K.W., Vigier, N., 2012. Lithium isotopes as tracers in marine and terrestrial environments. Handbook of Environmental Isotope Geochemistry. Springer Berlin Heidelberg, pp. 41–59.
Cerling, T.E., Solomon, D.K., Quade, J., Borman, J.R., 1991. On the isotopic composition of carbon in soil carbon dioxide. Geochim. Cosmochim. Acta 55, 3403–3405.
Cenki-Tok, B., Chabaux, F., Lemarchand, D., Schmitt, A.-D., Pierret, M.-C., Viville, D., Bagard, M.-L., Stille, P., 2009. The impact of water-rock interactions and vegetation on calcium

Please cite this article as: Sullivan, P.L., et al., CZ-tope at Susquehanna Shale Hills CZO: Synthesizing multiple isotope proxies to elucidate Critical Zone processes across timescal..., Chem. Geol. (2016), http://dx.doi.org/10.1016/j.chemgeo.2016.05.012

isotope fractionation in soil- and stream waters of a small, forested catchment (the Strengbach case). Geochim. Cosmochim. Acta 73, 2215–2228.
Chabaux, F., Bourdon, B., Riotte, J., 2008. U-series geochemistry in weathering profiles, river waters and lakes. Radioact. Environ. 13, 49–104.
Chabaux, F., Ma, L., 2011. Determination of chemical weathering rates from U series nuclides in soils and weathering profiles: Principles, applications and limitations. Appl. Geochem. S26, 20–23.
Chabaux, F., Blaes, E., Stille, P., di Chiara Roupert, R., Pelt, E., Dosseto, A., Brantley, S.L., 2013. Regolith formation rate from U-series nuclides: Implications from the study of a spheroidal weathering profile in the Rio Icacos watershed (Puerto Rico). Geochim. Cosmochim. Acta 100, 73–95.
Chadwick, O.A., Brimhall, G.H., Hendricks, D.M., 1990. From black box to a grey box: a mass balance interpretation of pedogenesis. Geomorphology 3, 369–390.
Chetelat, B., Gaillardet, J., Freydier, R., Négrel, P., 2005. Boron isotopes in precipitation: experimental constraints and field evidence from French Guiana. Earth Planet. Sci. Lett. 235, 16–30. http://dx.doi.org/10.1016/j.epsl.2005.02.014.
Chetelat, B., Liu, C.-Q., Gaillardet, J., Wang, Q.L., Zhao, Z.Q., Liang, C.S., Xiao, Y.K., 2009. Boron isotopes geochemistry of the Changjiang basin rivers. Geochim. Cosmochim. Acta 73, 6084–6097. http://dx.doi.org/10.1016/j.gca.2009.07.026.
Clark, I.D., Fritz, P., 1997. Environmental Isotopes in Hydrogeology. Lewis Publishers, New York, p. 328.
Cividini, D., Lemarchand, D., Chabaux, F., Boutin, R., Pierret, M.-C., 2010. From biological to lithological control of the B geochemical cycle in a forest watershed (Strengbach, Vosges). Geochim. Cosmochim. Acta 74, 3143–3163. http://dx.doi.org/10.1016/j.gca.2010.03.002.
Clarke, G.M., Ciolkosz, E.J., 1988. Periglacial geomorphology of the Appalachian highlands and interior highlands south of the glacial border—a review. Geomorphology 1, 191–220.
Cloquet, C., Carignan, J., Libourel, G., 2006. Isotopic composition of Zn and Pb atmospheric depositions in an urban/Periurban area of northeastern France. Environ. Sci. Technol. 40, 6594–6660.
Cockburn, H.A.P., Summerfield, M.A., 2004. Geomorphological applications of cosmogenic isotope analysis. Prog. Phys. Geogr. 28, 1–42.
Cotter, E., and Inners, J., 1986. Silurian stratigraphy and sedimentology in the Huntingdon County area, *in* Sevon, W., eds, Guidebook for the 51st Annual Field Conference of Pennsylvania Geologists, Selected Geology of Bedford and Huntingdon Counties: Field Conference of Pennsylvania Geologists, Bureau of Topographic and Geologic Survey, p. 27-39.
Dawson, T.E., Ehleringer, J.R., 1991. Streamside trees that do not use stream water. Nature 350, 335–337.
de Souza, G.F., Reynolds, B.C., Kiczka, M., Bourdon, B., 2010. Evidence for mass-dependent isotopic fractionation of strontium in a glaciated granitic watershed. Geochim. Cosmochim. Acta 74, 2596–2614.
Dellinger, M., Gaillardet, J., Bouchez, J., Calmels, D., Louvat, P., Dosseto, A., ... Maurice, L., 2015. Riverine Li isotope fractionation in the Amazon River basin controlled by the weathering regimes. Geochim. Cosmochim. Acta 164, 71–93.
Delvigne, C., Opfergelt, S., Cardinal, D., Delvaux, B., Andre, L., 2009. Distinct silicon and germanium pathways in the soil-plant system: evidence from banana and horsetail. J. Geophys. Res. Biogeosci. 114, G02013. http://dx.doi.org/10.1029/2008JG000899.
Derry, L.A., Kurtz, A.C., Ziegler, K., Chadwick, O.A., 2005. Biological control of terrestrial silica cycling and export fluxes to watersheds. Nature 433, 728–731.
Dosseto, A., Buss, H.L., Suresh, P.O., 2012. Rapid regolith formation over volcanic bedrock and implications for landscape evolution. Earth Planet. Sci. Lett. 337, 47–55.
Drivas, P., Bowers, T., Yamartino, R., 2011. Soil mixing depth after atmospheric deposition. I. Model development and validation. Atmos. Environ. 45 (25), 4133–4140.
Druhan, J.L., Maher, K., 2014. A model linking stable isotope fractionation to water flux and transit times in heterogeneous porous media. Procedia Earth Planet. Sci. 10, 179–188.
Druhan, J.L., Steefel, C.I., Molins, S., Williams, K.H., Conrad, M.E., DePaolo, D.J., 2012. Timing the onset of sulfate reduction over multiple subsurface acetate amendments by measurement and modeling of sulfur isotope fractionation. Environ. Sci. Technol. 46, 8895–8902.
Druhan, J.L., Steefel, C.I., Williams, K.H., DePaolo, D.J., 2013. Calcium isotope fractionation in groundwater: molecular scale processes influencing field scale behavior. Geochim. Cosmochim. Acta 119, 93–116.
Druhan, J.L., Steefel, C.I., Conrad, M.E., DePaolo, D.J., 2014. A large column analog experiment of stable isotope variations during reactive transport: I. A comprehensive model of sulfur cycling and delta *S*-34 fractionation. Geochim. Cosmochim. Acta 124, 366–393.
Dudka, S., Adriano, D.C., 1997. Environmental impacts of metal ore mining and processing: a review. J. Environ. Qual. 26, 590–602.
Eggert, G.G., 1994. The Iron Industry in Pennsylvania (No. 25). Pennsylvania Historical Association.
Ehleringer, J.R., Dawson, T.E., 1992. Water uptake by plants: perspectives from stable isotope composition. Plant Cell Environ. 15, 1073–1082.
Evans, M.J., Derry, L.A., 2002. Quartz control of high germanium-silicon ratios in geothermal waters. Geology 30, 1019–1022.
Evaristo, J., Jasechko, S., McDonnell, J.J., 2015. Global separation of plant transpiration from groundwater and streamflow. Nature 525, 91–93.
Fantle, M.S., Tipper, E.T., 2014. Calcium isotopes in the global biogeochemical Ca cycle: Implications for development of a Ca isotope proxy. Earth Sci. Rev. 129, 148–177.
Farkas, J., Dejeant, A., Novak, M., Jacobsen, S.B., 2011. Calcium isotope constraints on the uptake and sources of Ca^{2+} in a base-poor forest: a new concept of combining stable (delta Ca-44/42) and radiogenic (epsilon(Ca)) signals. Geochim. Cosmochim. Acta 75 (22), 7031–7046.
Flueckinger, L.A., 1969. Geology of a portion of the Allensville quadrangle, Centre and Huntingdon counties, Pennsylvania. Progress Report 176: Commonwealth of Pennsylvania, State Planning Board. Bureau of Topographic and Geologic Survey.
Gaines, K.P., Stanley, J.W., Meinzer, F.C., McCulloh, K.A., Woodruff, D.R., Chen, W., Adams, T.S., Lin, H., Eissenstat, D.M., 2015. Reliance on shallow soil water in a mixed-hardwood forest in Central Pennsylvania. Tree Physiol. (p.tpv113).
Galy, A., Bar-Matthews, M., Halicz, L., O'Nions, R.K., 2002. Mg isotopic composition of carbonate: insight from speleothem formation. Earth Planet. Sci. Lett. 201 (1), 105–115.
Galloway, J.N., Thornton, J.D., Norton, S.A., Volchok, H.L., McLean, R.A.N., 1982. Trace metals in atmospheric deposition: a review and assessment. Atmos. Environ. 16, 1677–1700.
Goldsmith, G.R., Muñoz-Villers, L.E., Holwerda, F., McDonnell, J.J., Asborsen, H., Dawson, T.E., 2012. Stable isotopes reveal linkages among ecohydrological processes in a seasonally dry tropical montane cloud forest. Ecohydrology 5, 779–790.
Graustein, W.C., Armstrong, R.L., 1983. The use of 87Sr/86Sr to measure atmospheric transport into forested watersheds. Science 219, 289–292.
Guelke, M., Von Blanckenburg, F., 2007. Fractionation of stable iron isotopes in higher plants. Environ. Sci. Technol. 41, 1896–1901.
Guelland, K., Hagedorn, F., Smittenberg, R.H., Göransson, H., Bernasconi, S.M., Hajdas, I., Kretzschmar, R., 2013. Evolution of carbon fluxes during initial soil formation along the forefield of Damma glacier, Switzerland. Biogeochemistry 113, 545–561.
He, Q., Walling, D.E., 1997. The distribution of fallout 137 Cs and 210 Pb in undisturbed and cultivated soils. Appl. Radiat. Isot. 48 (5), 677–690.
Heimsath, A.M., Dietrich, W.E., Nishiizumi, K., Finkel, R.C., 1997. The soil production function and landscape equilibrium. Nature 388, 358–361.
Herndon, E.M., Jin, L., Brantley, S.L., 2011. Soils reveal widespread manganese enrichment from industrial inputs. Environ. Sci. Technol. 45 (1), 241–247.
Hindshaw, R.S., Reynolds, B.C., Wiederhold, J.G., Kretzschmar, R., Bourdon, B., 2011. Calcium isotopes in a proglacial weathering environment: Damma glacier, Switzerland. Geochim. Cosmochim. Acta 75, 106–118.
Hindshaw, R.S., Reynolds, B.C., Wiederhold, J.G., Kiczka, M., Kretzschmar, R., Bourdon, B., 2013. Calcium isotope fractionation in alpine plants. Biogeochemistry 112, 373–388.
Huh, Y., Chan, L.H., Zhang, L., Edmond, J.M., 1998. Lithium and its isotopes in major world rivers: Implications for weathering and the oceanic budget. Geochim. Cosmochim. Acta 62, 2039–2051.
Huh, Y., Chan, L.H., Chadwick, O.A., 2004. Behavior of lithium and its isotopes during weathering of Hawaiian basalt. Geochem. Geophys. Geosyst. 5.
Jin, L., Andrews, D.M., Holmes, G.H., Lin, H., Brantley, S.L., 2011. Opening the "black box": water chemistry reveals hydrological controls on weathering in the Susquehanna Shale Hills Critical Zone Observatory. Vadose Zone J. 10, 928–942.
Jin, L., Brantley, S.L., 2011. Soil chemistry and shale weathering on a hillslope influenced by convergent hydrologic flow regime at the Susquehanna/Shale Hills critical zone observatory. Appl. Geochem. 26, S51–S56.
Jin, L., Ravella, R., Ketchum, B., Bierman, P.R., Heaney, P., White, T., Brantley, S.L., 2010. Mineral weathering and elemental transport during hillslope evolution at the Susquehanna/Shale Hills critical zone observatory. Geochim. Cosmochim. Acta 74, 3669–3691.
Jin, L., Ogrinc, N., Hamilton, S.K., Szrmek, K., Kanduc, T., Walter, L.M., 2009. Inorganic carbon isotope systematics in soil profiles undergoing silicate and carbonate weathering (Southern Michigan, USA). Chem. Geol. 264, 139–153.
Jin, L., Ogrinc, N., Yesavage, T., Hasenmuller, E.A., Ma, L., Sullivan, P.L., Kaye, J., Duffy, C., Brantley, S.L., 2014. The CO2 consumption potential during gray shale weathering: insights from the evolution of carbon isotopes in the Susquehanna Shale Hills critical zone observatory. Geochim. Cosmochim. Acta 142, 260–280.
Karim, A., Veizer, J., 2000. Weathering processes in the Indus River Basin: implications from riverine carbon, sulfur, oxygen and strontium isotopes. Chem. Geol. 170, 153–177.
Kendall, C., Caldwell, E.A., 1998. Fundamentals of isotope geochemistry. In: Kendall, C., McDonnell, J.M. (Eds.), Isotope tracers in catchment hydrology. Elsevier, Oxford, pp. 51–86.
Kaste, J.M., Heimsath, A.M., Bostick, B.C., 2007. Short-term soil mixing quantified with fallout radionuclides. Geology 35 (3), 243–246.
Kendall, C., Doktor, D.H., 2003. Stable isotope applications in hydrologic studies. In: Drever, J.I. (Ed.), Treatise on Geochemistry, Volume 5, Surface and Groundwater, Weathering, and Soil. Elsevier Pergamon, pp. 319–364.
Kendall, C., McDonnell, J.J., 2006. Isotope Tracers in Catchment Hydrology. Elsevier BV, Netherlands, Amsterdam.
Kennedy, M.J., Chadwick, O.A., Vitousek, P.M., Derry, L.A., Hendricks, D.M., 1998. Changing sources of base cations during ecosystem development, Hawaiian islands. Geology 26 (11), 1015–1018.
Kiczka, M., Wiederhold, J.G., Kraemer, S.M., Bourdon, B., Kretzschmar, R., 2010. Iron isotope fractionation during Fe uptake and translocation in alpine plants. Environ. Sci. Technol. 44, 6144–6150.
Kiczka, M., Wiederhold, J.G., Frommer, J., Voegelin, A., Kraemer, S.M., Bourdon, B., Kretzschmar, R., 2011. Iron speciation and isotope fractionation during silicate weathering and soil formation in an alpine glacier forefield chronosequence. Geochim. Cosmochim. Acta 75, 5559–5573.
Kirchner, J.W., 2003. A double paradox in catchment hydrology and geochemistry. Hydrol. Process. 17, 871–874.
Komarek, M., Ettler, V., Chrastny, V., Mihaljevic, M., 2008. Lead isotopes in environmental sciences: a review. Environ. Int. 34, 562–577.
Kraepiel, A.M.L., Dere, A.L., Herndon, E.M., Brantley, S.L., 2015. Natural and anthropogenic processes contributing to metal enrichment in surface soils of Central Pennsylvania. Biogeochemistry 123, 265–283.
Kurtz, A.C., Derry, L.A., Chadwick, O.A., 2002. Germanium-silicon fractionation in the weathering environment. Geochim. Cosmochim. Acta 66, 1525–1537.

Please cite this article as: Sullivan, P.L., et al., CZ-tope at Susquehanna Shale Hills CZO: Synthesizing multiple isotope proxies to elucidate Critical Zone processes across timescal..., Chem. Geol. (2016), http://dx.doi.org/10.1016/j.chemgeo.2016.05.012

Kurtz, A.C., Lugolobi, F., Salvucci, G., 2011. Germanium-silicon as a flow path tracer: application to the Rio Icacos watershed. Water Resour. Res. 47.

La Rocha, D., Brzezinski, C.M.A., DeNiro, M.J., 1997. Fractionation of silicon isotopes by marine diatoms during biogenic silica formation. Geochim. Cosmochim. Acta 61, 5051–5056.

Ladouche, B., Probst, A., Viville, D., Idir, S., Baqué, D., Loubet, M., Probst, J.-L., Bariac, T., 2001. Hydrograph separation using isotopic, chemical and hydrological approaches (Strengbach catchment, France). J. Hydrol. 242, 255–274.

Lantzy, R.J., Mackenzie, F.T., 1979. Atmospheric trace metals: global cycles and assessment of man's impact. Geochim. Cosmochim. Acta 43, 511–525.

Lemarchand, D., Gaillardet, J., 2006. Transient features of the erosion of shales in the Mackenzie basin (Canada), evidences from boron isotopes. Earth Planet. Sci. Lett. 245, 174–189. http://dx.doi.org/10.1016/j.epsl.2006.01.056.

Lemarchand, E., Schott, J., Gaillardet, J., 2005. Boron isotopic fractionation related to boron sorption on humic acid and the structure of surface complexes formed. Geochim. Cosmochim. Acta 69, 3519–3533 (doi:16/j.gca.2005.02.024).

Lemarchand, E., Schott, J., Gaillardet, J., 2007. How surface complexes impact boron isotope fractionation: evidence from Fe and Mn oxides sorption experiments. Earth Planet. Sci. Lett. 260, 277–296. http://dx.doi.org/10.1016/j.epsl.2007.05.039.

Lemarchand, E., Chabaux, F., Vigier, N., Millot, R., Pierret, M., 2010. Lithium isotope systems in a forested granitic catchment (Strengbach, Voseges Mountains, France). Geochim. Cosmochim. Acta 74, 4612–4628.

Li, L., Maher, K., Navarre-Sitchler, A., Druhan, J., Lawrence, C., Meile, C., Moore, J., Perdial, J., Sullivan, P.L., Thompson, A., Jin, L., Bolton, E., Brantley, S., Dietrich, W., Mayer, U., Steefel, C.I., Valocchi, A., Zachara, J., Kocar, B., Mcintosh, J., Tutolo, B.M., Beisman, J., Kumar, M., Sonnethal, E., 2016. Expanding the role of reactive transport modeling in earth surface processes. Geochim. Cosmochim. Acta.

Likens, G.E., Driscoll, C.T., Buso, D.C., Mitchell, M.J., Lovett, G.M., Bailey, S.W., Siccama, T.G., Reiners, W.A., Alewell, C., 2002. The biogeochemistry of sulfur at Hubbard Brook. Biogeochemistry 60, 235–316.

Lin, H., Zhou, X., 2008. Evidence of subsurface preferential flow using soil hydrologic monitoring in the Shale Hills catchment. Eur. J. Soil Sci. 59, 34–49.

Lin, H.S., Kogelmann, W., Walker, C., Bruns, M.A., 2006. Soil moisture patterns in a forested catchment: a hydropedological perspective. Geoderma 131, 345–368. http://dx.doi.org/10.1016/j.geoderma.2005.03.013.

Lloret, E., Dessert, C., Gaillardet, J., Albéric, P., Crispi, O., Chaduteau, C., Benedetti, M.F., 2011. Comparison of dissolved inorganic and organic carbon yields and fluxes in the watersheds of tropical volcanic islands, examples from Guadeloupe (French West Indies). Chem. Geol. 280, 65–78.

Louvat, P., Gaillardet, J., Paris, G., Dessert, C., 2011. Boron isotope ratios of surface waters in Guadeloupe, Lesser Antilles. Appl. Geochem. 26, S76–S79.

Ma, L., Chabaux, F., Pelt, E., Blaes, E., Jin, L., Brantley, S., 2010. Regolith production rates calculated with uranium-series isotopes at Susquehanna/Shale Hills critical zone observatory. Earth Planet. Sci. Lett. 297, 211–225.

Ma, L., Chabaux, F., Pelt, E., Granet, M., Sak, P.B., Gaillardet, J., Lebedeva, M., Brantley, S.L., 2012. The effects of curvature on weathering rind formation: evidence from U-series isotopes in basaltic andesite weathering clasts in Guadeloupe. Geochim. Cosmochim. Acta 80, 92–107.

Ma, L., Chabaux, F., West, N., Kirby, E., Jin, L., Brantley, S., 2013. Regolith production and transport in the Susquehanna Shale Hills critical zone observatory, part 1: insights from U-series isotopes. J. Geophys. Res. Earth Surf. 118, 722–740. http://dx.doi.org/10.1002/jgrf.20037.

Ma, L., Konter, J., Herndon, E., Jin, L., Steinhoefel, G., Sanchez, D., Brantley, S., 2014. Quantifying an early signature of the industrial revolution from lead concentrations and isotopes in soils of Pennsylvania, USA. Antaeus 7, 16–29.

Ma, L., Teng, F.Z., Jin, L., Ke, S., Yang, W., Gu, H.O., Brantley, S.L., 2015. Magnesium isotope fractionation during shale weathering in Shale Hills critical zone observatory: accumulation of light Mg isotopes in the soils by clay mineral transformation. Chem. Geol. 397, 37–50.

Maher, K., DePaolo, D.J., Christensen, J.N., 2006. U-Sr isotopic speedometer: fluid flow and chemical weathering rates in aquifers. Geochim. Cosmochim. Acta 70, 4417–4435.

Matisoff, G., Whiting, P.J., 2011. Handbook of environmental isotope geochemistry. In: Baskaran, M. (Ed.), Handbook of Environmental Isotope Geochemistry. Springer, Berlin Heidelberg, Berlin, Heidelberg, pp. 487–520.

McKean, J.A., Dietrich, W.E., Finkel, R.C., Southon, J.R., Caffee, M.W., 1993. Quantification of soil production and downslope creep rates from cosmogenic ^{10}Be accumulations on a hillslope profile. Geology 21, 343–346.

McDonnell, J.J., 2014. The two water worlds hypothesis: ecohydrological separation of water between streams and trees? WIREs Water 1, 323–329.

Meek, K., Derry, L.A., Cathles, L.M., Sparks, J., 2016. ^{87}Sr/86Sr, Ca/Sr, and Ge/Si ratios as tracers of solute sources and biogeochemical cycling at a temperate forested shale catchment, Huntingdon, Pennsylvania, USA. Chem. Geol. http://dx.doi.org/10.1016/j.chemgeo.2016.04.026.

Melton, E.D., Swanner, E.D., Behrens, S., Schmidt, C., Kappler, A., 2014. The interplay of microbially mediated and abiotic reactions in the biogeochemical Fe cycle. Nat. Rev. Microbiol. 12, 797–808.

Meredith, K., Moriguti, T., Tomascak, P., Hollins, S., Nakamura, E., 2013. The lithium, boron and strontium isotopic systematics of groundwaters from an arid aquifer system: implications for recharge and weathering processes. Geochim. Cosmochim. Acta 112, 20–31.

Michener, R., Lajtha, K. (Eds.), 2008. Stable Isotopes in Ecology and Environmental Science. John Wiley & Sons.

Monastra, V., Derry, L.A., Chadwick, O.A., 2004. Multiple sources of lead in soils from a Hawaiian chronosequence. Chem. Geol. 209, 215–231.

Navarre-Sitchler, A., Brantley, S.L., Rother, G., 2015. How porosity increases during incipient weathering of crystalline silicate rocks. Rev. Mineral. Geochem. 80, 331–354.

Noireaux, J., Gaillardet, J., Sullivan, P.L., Brantley, S.L., 2014. Boron isotope fractionation in soils at Shale Hill CZO. Procedia Earth Planet. Sci. 10, 218–222.

Nriagu, J.O., Pacyna, J.M., 1988. Quantitative assessment of worldwide contamination of air, water and soils by trace metals. Nature 333, 134–139.

Nutter, W.L., 1964. Determination of the Head-Discharge Relationship for a Sharp-Crested Compound Weir and a Sharp-Crested Parabolic Weir (Ph.D. diss.) Pennsylvania State University, University Park.

Oerter, E., Finstad, K., Schaefer, J., Goldsmith, G.R., Dawson, T., Amundson, R., 2014. Oxygen isotope fractionation effects in soil water via interaction with cations (Mg, Ca, K, Na) adsorbed to phyllosilicate clay minerals. J. Hydrol. 515, 1–9.

Opfergelt, S., Delmelle, P., 2012. Silicon isotopes and continental weathering processes: assessing controls on Si transfer to the ocean. Compt. Rendus Geosci. 344, 723–738.

Opfergelt, S., Georg, R.B., Delvaux, B., Cabidoche, Y.-M., Burton, K.W., Halliday, A.N., 2012a. Mechanisms of magnesium isotope fractionation in volcanic soil weathering sequences, Guadeloupe. Earth Planet. Sci. Lett. 341–344, 176–185.

Opfergelt, S., Georg, R.B., Delvaux, B., Cabidoche, Y.-M., Burton, K.W., Halliday, A.N., 2012b. Silicon isotopes and the tracing of desilication in volcanic soil weathering sequences, Guadeloupe. Chem. Geol. 326 –327, 113–122.

Pavich, M.J., Brown, L., Harden, J., Klein, J., Middleton, R., 1986. ^{10}Be distribution in soils from Merced River terraces, California. Geochim. Cosmochim. Acta 50, 1727–1735.

Page, B.D., Bullen, T.D., Mitchell, M.J., 2008. Influences of calcium availability and tree species on Ca isotope fractionation in soil and vegetation. Biogeochemistry 88 (1), 1–13.

Pett-Ridge, J.C., Monastra, V.M., Derry, L.A., Chadwick, O.A., 2007. Importance of atmospheric inputs and Fe-oxides in controlling soil uranium budgets and behavior along a Hawaiian chronosequence. Chem. Geol. 244, 691–707.

Pett-Ridge, J.C., Derry, L.A., Barrows, J.K., 2009a. Ca/Sr and 87Sr/86Sr ratios as tracers of Ca and Sr cycling in the Rio Icacos watershed, Luquillo Mountains, Puerto Rico. Chem. Geol. 267, 32–45.

Pett-Ridge, J.C., Derry, L.A., Kurtz, A.C., 2009b. Sr isotopes as a tracer of weathering processes and dust inputs in a tropical granitoid watershed, Luquillo Mountains, Puerto Rico. Geochim. Cosmochim. Acta 73, 25–43.

Pierret, M.C., Stille, P., Prunier, J., Viville, D., Chabaux, F., 2014. Chemical and U–Sr isotopic variation in stream and sources waters of the Strengbach watershed (Vosges mountains, France). Hydrol. Earth Syst. Sci. 18, 3969–3985.

Pistiner, J.S., Henderson, G.M., 2003. Lithium-isotope fractionation during continental weathering processes. Earth Planet. Sci. Lett. 214, 327–339.

Poreba, G.J., 2006. Caesium-137 as a soil erosion tracer: A review. Geochronometria 25, 37–46.

Probst, A., Gh'mari, A.E., Aubert, D., Fritz, B., McNutt, R., 2000. Strontium as a tracer of weathering processes in a silicate catchment polluted by acid atmospheric inputs, Strengbach, France. Chem. Geol. 170, 203–219.

Qu, Y., Duffy, C.J., 2007. A semidiscrete finite volume formulation for multiprocess watershed simulation. Water Resour. Res. 43, W08419.

Raab, T., Leopold, M., Völkel, J., 2007. Character, age, and ecological significance of Pleistocene periglacial slope deposits in Germany. Phys. Geogr. 28, 451–473.

Rauch, J.N., Pacyna, J.M., 2009. Earth's global Ag, Al, Cr, Cu, Fe, Ni, Pb, and Zn cycles. Glob. Biogeochem. Cycles 23, GB2001. http://dx.doi.org/10.1029/2008GB003376.

Rempe, D.M., Dietrich, W.E., 2014. A bottom-up control on fresh-bedrock topography under landscapes. Proc. Natl. Acad. Sci. U. S. A. 111, 6576–6581.

Reuer, M.K., Weiss, D.J., 2002. Anthropogenic lead dynamics in the terrestrial and marine environment. Philos. Trans. R. Soc. Lond. A 360, 2889–2904.

Riotte, J., Chabaux, F., 1999. ^{243}U/^{238}U activity ratios in freshwaters as tracers of hydrological processes: the Strengbach watershed (Vosges, France). Geochim. Cosmochim. Acta 63, 1263–1275.

Rive, K., Gaillardet, J., Agrinier, P., Rad, S., 2013. Carbon isotopes in the rivers from the Lesser Antilles: origin of the carbonic acid consumed by weathering reactions in the lesser Antilles. Earth Surf. Process. Landf. 38, 1020–1035.

Rose, E.F., Chaussidon, M., France-Lanord, C., 2000. Fractionation of boron isotopes during erosion processes: the example of Himalayan rivers. Geochim. Cosmochim. Acta 64, 397–408. http://dx.doi.org/10.1016/S0016-7037(99)00117-9.

Roy, S., Négrel, P., 2001. A Pb isotope and trace element study of rainwater from the Massif Central (France). Sci. Total Environ. 277, 225–239.

Schaller, M., von Blanckenburg, F., Veit, H., Kubik, P., 2003. Influence of periglacial cover beds on in situ-produced cosmogenic Be-10 in soil sections. Geomorphology 49, 255–267.

Schlosser, P., Stute, M., Dörr, H., Sonntag, C., Münnich, K.O., 1988. Tritium/3 He dating of shallow groundwater. Earth Planet. Sci. Lett. 89, 353–362.

Schmitt, A.-D., Vigier, N., Lemarchand, D., Millot, R., Stille, P., Chabaux, F., 2012. Processes controlling the stable isotope compositions of Li, B, Mg and Ca in plants, soils and waters: a review. Compt. Rendus Geosci. 344, 704–722.

Scholl, M.A., Shanley, J.B., Murphy, S.F., Willenbring, J.K., Occhi, M., González, G., 2015. Stable-isotope and solute-chemistry approaches to flow characterization in a forested tropical watershed, Luquillo Mountains, Puerto Rico. Appl. Geochem.

Sebilo, M., Mayer, B., Nicolardot, B., Pinay, G., Mariotti, A., 2013. Long-term fate of nitrate fertilizer in agricultural soils. Proc. Natl. Acad. Sci. 110, 18185–18189.

Shi, Y., Davis, K.J., Duffy, C.J., Yu, X., 2013. Developing a couple land surface hydrologic model and evaluation at a critical zone observatory. J. Hydrometeorol. 14, 1401–1420.

Spivack, A.J., Palmer, M.R., Edmond, J.M., 1987. The sedimentary cycle of the boron isotopes. Geochim. Cosmochim. Acta 51, 1939–1949.

Stallard, R.F., 1992. Tectonic processes, continental freeboard, and the rate-controlling step for continental denudation. In: Butcher, S.S., Charlson, R.J., Orians, G.H., Wolfe, G.V. (Eds.), Global Biogeochemical Cycles. Academic Press, London, pp. 93–121.

Strauss, H., 1999. Geological evolution from isotope proxy signals sulfur. Chem. Geol. 161, 89–101.

Please cite this article as: Sullivan, P.L., et al., CZ-tope at Susquehanna Shale Hills CZO: Synthesizing multiple isotope proxies to elucidate Critical Zone processes across timescal..., Chem. Geol. (2016), http://dx.doi.org/10.1016/j.chemgeo.2016.05.012

Sullivan, P.L., Hynek, S., Gu, X., Singha, K., White, T., West, N., Kim, H., Clarke, B., Kirby, E., Duffy, C.J., Brantley, S.L., et al., 2016. Oxidative dissolution at the channel leads geomorphological evolution at the Shale Hills Catchment. Am. J. Sci. (in revision).

Stewart, B.W., Capo, R.C., Chadwick, O.A., 2001. Effects of rainfall on weathering rate, base cation provenance, and Sr isotope composition of Hawaiian soils. Geochim. Cosmochim. Acta 65, 1087–1099.

Tamburini, F., Pfahler, V., Bünemann, E.K., Guelland, K., Bernasconi, S.M., Frossard, E., 2012. Oxygen isotopes unravel the role of microorganisms in phosphate cycling in soils. Environ. Sci. Technol. 46, 5956–5962.

Taylor, M.P., Hudson-Edwards, K.A., Mackay, A.K., Holz, E., 2010. Soil Cd, Cu, Pb and Zn contaminants around Mount Isa city, Queensland, Australia: potential sources and risks to human health. Appl. Geochem. 25 (6), 841–855.

Thomas, E.M., Lin, H., Duffy, C.J., Sullivan, P.L., Holmes, G.H., Brantley, S.L., Jin, L., 2013. Spatiotemporal patterns of water stable isotope compositions at the Shale Hills critical zone observatory: linkages to subsurface hydrologic processes. Vadose Zone Res. 40. http://dx.doi.org/10.2136/vzj2013.

Thompson, A., Ruiz, J., Chadwick, O.A., Titus, M., Chorover, J., 2007. Rayleigh fractionation of iron isotopes during pedogenesis along a climate sequence of Hawaiian basalt. Chem. Geol. 238, 72–83.

Tipper, E.T., Galy, A., Bickle, M.J., 2006. Riverine evidence for a fractionated reservoir of Ca and Mg on the continents: implications for the oceanic Ca cycle. Earth Planet. Sci. Lett. 247, 267–279.

Tipper, E.T., Lemarchand, E., Hindshaw, R.S., Reynolds, B.C., Bourdon, B., 2012. Seasonal sensitivity of weathering processes: hints from magnesium isotopes in a glacial stream. Chem. Geol. 312, 80–92.

Trumbore, S.E., 2000. Constraints on below-ground carbon cycling from radiocarbon: the age of soil organic matter and respired CO_2. Ecol. Appl. 10, 399–411.

Vengosh, A., Heumann, K.G., Juraske, S., Kasher, R., 1994. Boron isotope application for tracing sources of contamination in groundwater. Environ. Sci. Technol. 28, 1968–1974.

Vogel, J.C., 1993. Variability of carbon isotope fractionation during photosynthesis. In: Ehleringer, J.R., Hall, A.E., Farquhar, G.D. (Eds.), Stable Isotopes and Plant Carbon–Water Relations. Academic Press, San Diego, CA, pp. 29–38.

Viville, D., Ladouche, B., Bariac, T., 2006. Isotope hydrological study of mean transit time in the granitic Strengbach catchment (Vosges massif, France). Application of the FlowPC model with modified input function. Hydrol. Process. 20, 1737–1751.

Wadleigh, W.A., Schwarcz, H.P., Kramer, J.R., 1994. Sulphur isotope tests of seasalt correction factors in precipitation: Nova Scotia, Canada. Water Air Soil Pollut. 77, 1–16.

West, N., Kirby, E., Bierman, P., Slingerland, R., Ma, L., Rood, D., Brantley, S.L., 2013. Regolith production and transport at the Susquehanna Shale Hills critical zone observatory, part 2: insights from meteoric 10Be. J. Geophys. Res. Earth Surf. 118, 1877–1896. http://dx.doi.org/10.1002/jgrf.20121.

West, N., Kirby, E., Bierman, P., Clarke, B.A., 2014. Aspect-dependent variations in regolith creep revealed by meteoric ^{10}Be. Geology 43, 83–86.

White, A.F., Schulz, M.S., Vivit, D.V., Blum, A.E., Stonestrom, D.A., Harden, J.W., 2005. Chemical weathering rates of a soil chronosequence on granitic alluvium: III. Hydrochemical evolution and contemporary solute fluxes and rates. Geochim. Cosmochim. Acta 69, 1975–1996.

Wiegand, B.A., Chadwick, O.A., Vitousek, P.M., Wooden, J.L., 2005. Ca cycling and isotopic fluxes in forested ecosystems in Hawaii. Geophys. Res. Lett. 32.

Yesavage, T., Fantle, M.S., Vervoort, J., Mathur, R., Jin, L., Liermann, L., Brantley, S.L., 2012. Fe cycling in the Shale Hills critical zone observatory, Pennsylvania: an analysis of biogeochemical weathering and Fe isotope fractionation. Geochim. Cosmochim. Acta 99, 18–38.

Ziegler, K., Chadwick, O.A., White, A.F., Brzezinski, M.A., 2005. δ^{30}Si systematics in a granitic saprolite, Puerto Rico. Geology 33, 817–820.

Please cite this article as: Sullivan, P.L., et al., CZ-tope at Susquehanna Shale Hills CZO: Synthesizing multiple isotope proxies to elucidate Critical Zone processes across timescal..., Chem. Geol. (2016), http://dx.doi.org/10.1016/j.chemgeo.2016.05.012